University of North Dakota
UND Scholarly Commons

Chemical Engineering Faculty Publications | Department of Chemical Engineering

2021

Activated carbon in mixed-matrix membranes

Jeremy Lewis

Maram A. Q Al-sayaghi

Chris Buelke

Ali Alshami
University of North Dakota, ali.alshami@und.edu

How does access to this work benefit you? Let us know!

Follow this and additional works at: https://commons.und.edu/che-fac

Recommended Citation

Jeremy Lewis, Maram A. Q Al-sayaghi, Chris Buelke, et al.. "Activated carbon in mixed-matrix membranes" (2021). *Chemical Engineering Faculty Publications*. 26.
https://commons.und.edu/che-fac/26

This Article is brought to you for free and open access by the Department of Chemical Engineering at UND Scholarly Commons. It has been accepted for inclusion in Chemical Engineering Faculty Publications by an authorized administrator of UND Scholarly Commons. For more information, please contact und.commons@library.und.edu.

Activated carbon in mixed-matrix membranes

Jeremy Lewis, Maram A. Q. Al-sayaghi, Chris Buelke, Ali Alshami*
*Corresponding author ali.alshami@und.edu

Department of Chemical Engineering - University of North Dakota, Grand Forks, ND

1. Introduction 2
1.1 Motivation 2
1.2 Background 3
2. Production of Biochar and Activated Carbon 4
2.1 Pyrolysis 4
2.2 Biochar 5
2.3 Activated Carbon 5
2.4 Carbon Molecular Sieves 6
3. AC Compatibility with Polymers and Solvents 6
4. Fabrication of MMMs 8
4.1 Formation of Casting Solution 8
4.2 Membrane Casting 9
4.3 Phase Inversion 9
4.3.1 Wet Phase Inversion 9
4.3.2 Dry Phase Inversion 10
4.3.3 Dry/Wet Phase Inversion 11
5. Relationship Between Surface Chemistry and Permeability 11
6. Application of AC-MMMs 13
6.1 AC-MMM uses in Water Purification 13
6.1.1 Rejection of Heavy Metal Ions 13
6.1.2 Rejection of Uranium 14
6.1.3 Rejection of Aromatic Compounds 14
6.2 AC-MMM uses in Biological Solute Rejection 16
6.2.1 Removal of Organic Matter 16
6.2.2 *E. Coli.* Removal 17
6.2.3 Blood Plasma Toxin Removal 17
6.3 AC-MMM uses in Pervaporation 18
6.4 AC-MMM uses in Gas Separation 19
6.4.1 Small, Low Molecular Weight, Non-Polar Binary Mixtures 19
6.4.2 Higher Hydrocarbons 22
6.5 Proton Exchange AC-MMMs for a Direct Methanol Fuel Cell 23
7. Predictive Models 23
8. Suggestions for Future Work 28
9. Acknowledgements 29
10. References 29

Abbreviations

ABS	acetonitrile butadiene styrene	PBT	protein bound toxins
AC	activated carbon	PCS	p-cresylsulfate
CAP	cellulose acetate phthalate	PDMS	polydimethylsiloxane
CMS	carbon molecular sieves	PEBAX 2533	polyether block amide
CNF	cellulose nanofiber	PEG	polyethylene glycol
COD	chemical oxygen demand	PEI	polyethylenimine
CTA	cellulose triacetate	PES	polyethersulfone
E. coli	Escherichia coli	POMS	poly(octylmethylsiloxane)
FFV	fractional free volume	PPSU	polyphenylsulfone
GPG	Gonzo-Parentis-Gottifred	PSF	polysulfone
HA	hippuric acid	PVC	polyvinyl chloride
IS	indoxyl sulfate	PVP	polyvinylpyrrolidone
KH550	$NH_2(CH_2)_3Si(OC_2H_5)_3$	PWF	pure water flux
LMH	$Lm^{-2}h^{-1}$	SEM	scanning electron microscopy
MMM	mixed matrix membrane	U	uranium
PAC	powdered activated carbon	UV_{254}	measured by UV-Vis at 254 nm
PAE	polyamide-amine-epichlorohydrin	YDH-171	CH_2CH- $Si(OCH_3)_3$

Abstract

Mixed matrix membranes (MMMs) have emerged as strong contenders to conventional membranes for gas and liquid separations. Although numerous studies on filler/matrix combinations have been conducted and thoroughly reviewed, a review of activated carbon (AC) as a filler has thus far been minimal. This review intends to fill this gap via critically analyzing the state-of-the-art on AC as a filler in MMMs. Aspects of AC-MMM research, with emphasis on AC fabrication from biomass pyrolysis, AC-MMM fabrication and resulting properties, and influence of AC on MMM performance are thoroughly elucidated. Furthermore, the various applications that have been investigated with AC-MMM membranes, and several predictive models that have been specifically utilized for AC-MMMs are also discussed.

1. Introduction

1.1 Motivation

Membranes for liquid and gas phase separations have evolved considerably in the past few decades. One major breakthrough was the development of MMMs, which are a composite two-phase membrane consisting of a polymeric continuous phase and a dispersed organic or inorganic filler. The continuous phase is commonly referred to as the matrix. MMMs have been the subject of extensive research studies and reviews involving a variety of organic and inorganic fillers, except for AC and biochar: two significant fillers with promising separation properties coupled with an abundance of low-cost raw material and processing techniques.

In recent years, AC has been gaining traction as a filler in MMMs. In this work, we present an up-to-date review of the literature and the state-of-the-art of research involving MMMs with the primary focus on AC and biochar as principal fillers. Special emphasis will be directed towards addressing AC-MMMs in terms of its formation, properties, applications, and predictive models that can be utilized for their performance.

1.2 Background

Starting as early as 1973, MMMs were studied by Paul and Kemp (1) and have grown into a field of their own. In some sense, the term "mixed matrix membrane" is a broad category of composite membranes that consist of adsorbent, nanocomposite, and hybrid membranes. During the late 1970s, MMMs were referred to as sorbent membranes, because adsorbent fillers were originally used and their adsorbent properties exploited (1). Recently, MMMs have been cited as both nanocomposite membranes (2,3), especially when the filler is nanometers in diameter, and as hybrid membranes (4) which highlight the two species independently responsible for selectivity.

Nonetheless, MMMs remain attractive because by combining the properties of the matrix and filler, enhanced properties are achieved including improved separation performance in terms of selectivity and flux, as well as physiochemical properties such as hydrophilicity, porosity, surface charge, and mechanical strength.

Several different combinations of filler/matrix materials have been investigated. Commonly reported fillers include carbon nanotubes (5), metal organic frameworks (6), molecular sieve particles (7,8), and zeolites (9). A breadth of polymers have been studied in MMMs including polyimides (10,11), polysulfones (12,13,14), copolymers (15), and cellulose acetate (16) to name a few. Altogether, these combinations have been investigated for applications including water purification, pervaporation, gas separation, and proton exchange.

Many articles have been written reviewing the topic of MMMs in the last decade. Aroon et al. (17), Goh at al. (18), and Chung et al. (19) authored reviews focusing on gas phase separations. Rezakazemi and Vinoba et al. focused specifically on carbon dioxide separation (20,21). Goh et al. (22) and Qadir et al. (23) published reviews focusing on water purification. Other reviews focused specifically on filler materials including zeolites (9,24), metal organic frameworks (6), nanoparticles (25), and 2D materials (26,27).

Considering the breadth of matrix and filler materials as well as applications that have been investigated, one point of confusion in the definition of MMMs is the classification of the filler. Most reports in the literature define the filler as inorganic, while still recognizing organic type fillers as possibilities. For example, carbon nanotubes and graphene are two organic compounds (i.e. made of only C, H, N, O) that have been categorized as organic and inorganic. Thus, the confusion has arisen because of the somewhat arbitrary categorization of organic and inorganic materials, because polymers are typically referred to as organics, and due to filler materials behaving very differently than polymers.

A comparison of MMMs to different membranes is presented in Table 1. Note the different categories for polymeric and organic membranes. Categorizing membranes into these four classes helps alleviate some confusion, especially between organic, inorganic, and polymeric materials. Although it is not common practice to present the class of "organic membranes" to mean those such as graphene, it is the authors' opinion this categorization is useful.

2. Production of Biochar and Activated Carbon

Biochar primarily is the solid product of biomass pyrolysis and is commonly used as a precursor for AC, which is a unique material for various reasons. Variable particle sizes are achievable with simple mechanical grinding or crushing methods. AC is highly porous leading to excellent adsorptive capacity for various gaseous and aqueous species. They can also be functionalized by physical or chemical treatment, making them versatile for various applications.

2.1 Pyrolysis

AC is typically produced from carbonaceous materials such as biomass, sludge, and petroleum pitch via pyrolysis, a thermochemical decomposition of matter at a relatively moderate temperature range of 200 to 700 °C. Currently, commercial AC is produced from coconut husks, wood saw dust, and coal (36). The first step in producing AC is the formation of char from these carbonaceous materials.

Depending on the pyrolysis conditions and end use, char takes on different names. Ahmad et al. conducted a thorough review including the definitions used for the pyrolyzed carbonaceous materials (37). In essence, char from a biomass feedstock has been labeled as biochar when it is produced in a dry environment and used as a soil amendment. Hydrochar is produced from biomass in an aqueous environment. On the other hand, charcoal is produced from coal and is meant to be used as a fuel. In recent years, the term biochar has been used to convey solid-pyrolyzed biomass, regardless of its end use. For simplicity, this paper defines biomass in its traditional sense, and AC is any biochar or other precursor that is activated as described in the following section.

Two types of pyrolysis are frequently studied: fast and slow pyrolysis, with the principle difference between them being the heating rate. In fast pyrolysis, the heating rate is on the order of hundreds of degrees centigrade per second, reaching its maximum temperature within seconds. The heating rate of slow pyrolysis, on the other hand, is on the order of tens of degrees centigrade per minute, reaching a peak temperature after several minutes, hours, or days (38).

Reactions taking place during the pyrolysis of biomass have proven to be extremely complicated. Depending on the feedstock, various products are formed based upon processing temperature and residence time (39). Regardless of the chemical species formed, it is clear that the result of pyrolysis is four unique product mixtures: 1) volatile gases, 2) bio-oils, 3) tars, and 4) solid char. Previous studies have focused on maximizing yield and characterizing bio-oils (40). Bio-oils are potentially low grade fuel sources or fuel additives, as their heating values are typically slightly lower than conventional fuels (41). Tars are typically an undesired by-product of pyrolysis (42); however, some research has been conducted on upgrading their by-products into more desirable

compounds (43). There is also some potential in using the tar as a composite additive (44). The solid that remains post pyrolysis treatment is the biochar.

2.2 Biochar

Biochar produced in the aforementioned section has several beneficial physical properties. Most notably, various sized pores are formed that create a porous substructure with a large amount of surface area (45,46,47). Depending on the biomass feedstock and pyrolysis conditions, surface functional groups tend to form, influencing its hydrophobicity and wettability (48). Table 2 lists a wide range of biochar derived from various feedstock and their relevant resulting properties. For a detailed review on biochar formation mechanisms, properties, and how biochar functionalization occurs, see Liu et al. (49).

In general, there exists a tradeoff between surface area and functional group formation as pyrolysis temperature increases. At high pyrolysis temperatures, biomasses tend to break down into bulky aromatics and lose their oxygen containing functional groups, which leads to high surface area. At relatively low temperatures, biochars tend to retain their functional groups, but have lower surface area. At extremely high temperatures, thermal cracking of the biochar occurs, causing pores to collapse and decreasing surface area. Depending on the biomass, an optimal temperature can vary between 300-800°C.

2.3 Activated Carbon

Once biochars are formed, they are subjected to activation treatments including physical, chemical, or combination activation. The term 'activated' is most often used to describe the state of enhanced physical and functional properties.

Physical activation involves high-temperature treatment of biochar with oxidizing gases, such as carbon dioxide (63), steam (64), and air (65). Often physical activation leads to enhanced surface area and pore density while oxidizing surface functional groups. The formation of C=O and O-H functional groups are typically apparent, whereas C-H and C-O functional groups usually disappear.

Chemical activation involves first impregnating the biochar with a chemical compound and then subjecting it to a high temperature treatment in an inert atmosphere or a vacuum. Typical activating chemicals are acids, bases, and oxidizing agents such as zinc chloride or hydrogen peroxide (66). An important parameter to consider during chemical activation is the impregnation ratio, or the ratio of the activating agent to the biochar. Upon impregnation, the biochar is subsequently treated at elevated temperatures in an inert atmosphere. This step is most often referred to as carbonization. Following carbonization, the AC is typically washed with a weak acid or base to remove the residual activating agent, and then washed with distilled or deionized water. Chemical activation can lead to an increased surface area, pore size and volume, and tailored functional groups. Table 3 summarizes recent literature in terms of feedstock, activating methods, and resulting properties.

Chemical activation generally leads to the formation of carbonyl functional groups, such as ketones and carboxylic acids. The hydroxide functional group is also typically present, though in

varying degrees depending on precursor biomass. Another noteworthy trend commonly seen is a maximum surface area achieved with respect to an optimal carbonization temperature. At relatively low temperatures, pore formation is restricted while at relatively high temperatures, functional groups tend to collapse and reduce pore size. Both scenarios result in lower specific surface areas. It is also apparent that the higher the impregnating ratio, the higher the specific surface area becomes for any one activating chemical at a specified temperature. Other factors such as carbonization pretreatment and chemical washing of the AC tend to also influence the final properties.

Due to ACs having large surface areas, pore volume, and functionality, they adsorb species from both liquids and gases. Hence, regardless the type of fluid under investigation, liquid or gas, it is necessary to consider the adsorption of each species onto the AC to fully exploit and understand the separation capabilities of AC-MMMs.

2.4 Carbon Molecular Sieves

CMS are a class of AC which are derived from polymeric precursors rather than biomass. Despite the difference in precursors, CMS are fabricated and activated in a manner very similar to that of AC. This is by controlled pyrolysis and further chemical or physical activation (77). There are a couple very important differences between CMS and AC. First is the resulting pore sizes after pyrolysis. CMS typically contain pore sizes in the micropore and ultramicropore range (77), while AC typically have a broad pore size distribution in the micro, meso, and macro pore region (78,79). Secondly, CMS can be directly prepared into membranes. For instance, a cast membrane can undergo pyrolysis and retain its shape, resulting in CMS membranes, or simply, carbon membranes (80). Although an interesting class of membrane, carbon membranes are not included in this review. Rather, CMS can be made into particles, by mechanical grinding, and used as a filler in MMMs (81). These types of materials are discussed where appropriate.

3. AC Compatibility with Polymers and Solvents

The interaction of AC with both the polymer phase and solvent play an important role in AC-MMM development. One issue is sedimentation, whereby particles tend to settle in the casting solution rather than form a suspension. This is an occurrence that challenges the use of many fillers, and notably AC, in MMMs (82). Sedimentation causes undesired variability in particle loading, and skewed particle size distribution in the final membranes. To avoid separation from casting solutions, particle size should be closely controlled as small particles generally remain suspended in the solution longer (15). Another method is to ensure adequate mixing with sonication, albeit partial sedimentation may occur in some solvents (83).

A secondary issue that usually arises from improper solvent selection is particle breakage, in which some solvents possess the capability of etching formed pores in AC (84). This causes breakage as depicted in Figure 1. Although the breakage of AC in solvent is not frequently considered, the reduction in particle size and pore volume are two possible results that could cause unforeseen effects to AC-MMMs.

The most prominent issue with MMMs, however, remains to be the poor polymer-filler interaction causing unselective void space and consequently unselective membranes (6,24,85,86). While there

is generally a good understanding of how some particles, such as colloids (87), interact in various solutions, very little is thus far known about the exact AC-polymer interaction. It has been suggested that the adsorption capacity of polymers by AC can be a good metric for compatibility (88); nevertheless, this has only been investigated for water soluble polymers in the liquid phase and not with interactions between two solid phases (88). Currently, photographic and thermomechanical observations serve as the best metric for AC/polymer compatibility.

Imaging is sometimes used to observe adhesion between AC particles and the polymer within the cross section of MMMs (89). Although not accurate, thin polymeric coatings surrounding AC particles can indicate good compatibility. In terms of mechanical properties, when a specific AC is compatible with the polymer matrix, mechanical properties tend to improve as measured by increases in tensile strength (90), fracture stress (91), or Young's modulus (90). Thermal properties also tend to become enhanced, as measured by an increase in glass transition temperature (92,93).

Loading MMMs with AC of small particle size is one method to increase interaction (94). For example, AC with a particle size of 750 nm demonstrated good interaction in a CAP matrix as measured by an increase in fracture stress (91). Particles with sizes between 1.5 and 3.5 micron showed good compatibility with a POMS matrix (89). However, it has been shown that, not only does the average size influence AC/polymer interaction, but the size distribution does as well. AC with a larger particle size distribution tend to disperse in a more inhomogeneous fashion and agglomerate more frequently (89).

Other methods to improve polymer-filler interaction include utilizing AC that has similar hydrophobicity or hydrophilicity as the polymer (95), which enables the binding of the polymer to the AC particles and increases the likelihood of strong interfacial compatibility (85).

The incorporation of ionic liquid additives into the MMM has also shown to improve the compatibility of filler/matrix (96). Ionic liquids act as a wetting agent between the particle and matrix, preventing the formation of interfacial defects. Moreover, the use of ionic liquid additives can prove versatile, as various anion/cation combinations are possible and can be tailored to specific membranes or applications (97). Surfactant and other salt additives also serve to improve the filler/matrix interaction by maintaining a particle suspension, preventing particle agglomeration and subsequent sedimentation. Other low molecular weight additives can serve to physically fill the void space between filler and matrix, improving the MMM performance (98).

The influence of functional groups is one of the most important factors to consider. Poor intermolecular interactions between filler and matrix is the ultimate cause of interfacial defects. Thus, much worked has been performed in fabricating and modifying fillers to improve this interaction (98). Strong intermolecular forces like hydrogen bonding and dipole interactions are prime targets. However, pi-pi stacking of highly aromatic fillers or matrixes can also contribute to strong interaction (11). Various methods have been performed to achieve the desired functional groups on fillers in MMMs. Grafting of various molecules such as silane coupling agents is a well-accepted method, specifically for zeolites, silica, and carbonaceous fillers. Functional groups can also be directly incorporated onto fillers by surface modifications. Variations in synthesis conditions with additives is especially effective at creating multifunctional sites on metal organic frameworks. Ion exchange treatment can also be performed to alter ionic sites to the filler (98).

AC presents an interesting case for functional group led design of MMMs. As discussed earlier and shown in table 2 and 3, the functional groups present in AC is dependent on precursor and activating method. Thus it is important to carefully consider the AC precursor and the parameters that are chosen to create the AC, due to their influence on functional groups. Other, yet more involved, methods for adding functionality and improving interfacial compatibility of AC have been investigated. For example, Saranya et al. functionalized AC with alginate to form AC-alginate aggregates, and then further cross-linked the aggregates with calcium as shown in Figure 2 (99). The alginate functionalized AC ensured active adsorption sites were available and prevented AC agglomeration.

Another method of modifying AC to enhance its interaction with polymers is by grafting silane coupling agents. Lan et al. grafted two different compounds, YDH-171 and KH550, to biochar (Fig. 3) (95). By grafting with hydrophobic or hydrophilic compounds, the overall hydrophobicity of the MMMs could be altered or enhanced. In this case, YDH-171 in a PDMS matrix resulted in MMMs with higher hydrophobicity than pristine PDMS (95).

4. Fabrication of MMMs

MMMs are fabricated into two primary configurations: flat sheets and hollow fibers. Depending upon the desired end application, membrane thicknesses can range between 10 – 200 microns, and can have active layers less than 10 microns. Both flat sheets and hollow fiber membranes can be formed in a similar fashion: casting solution formation, casting, and then precipitation. Each step is detailed in the following sections.

4.1 Formation of Casting Solution

Several methods exist to formulate the casting solution (94). The simplest one is by simultaneously dissolving the polymer and the AC in the appropriate solvent. Although quick and simple, this method runs the risk of disrupting the polymeric chains and forming agglomerations. A slightly different, but more common method, involves first dissolving the polymer in the solvent, then adding the AC once the polymer is completely dissolved (15,90). While this reduces the risk of disrupting the polymer chains, AC agglomerations may still form. In order to further reduce the risk of possible agglomeration, some researchers have dissolved the polymer and AC in a solvent separately, then combined the two solutions (89,100,101). Another method to reduce the presence of agglomerations in the casting solution is to simply filter it using a fine mesh before casting (15,102). In doing so, the casting solution is separated from agglomerates with a larger size than the mesh utilized. For all methods, dispersion of the filler in the solvent and the polymer is facilitated by mechanical stirring. Although polymer solutions are viscous, sonication can further disperse the filler and eliminate trapped gases without degrading the polymer (103,104).

The concentration of the polymer in the casting solution, as well as the choice of solvent, are critical parameters influencing pore size, thickness, free volume, d-spacing, and ultimately the separation properties of the formed membrane (105,106,107). One of the most crucial parameters for MMMs is the amount of filler added. That is, dilute amounts of filler can have negligible influences on membrane properties, and high concentrations of filler tend to cause void formation, agglomeration and surface ruptures.

4.2 Membrane Casting

Once the casting solution is made, it can then be formed into the desired shape. Most commonly, flat sheet membranes are cast using a casting knife or doctor blade on a proper supporting material made of glass or other rigid and inert materials (108). A moderate casting speed is usually utilized ranging from 2 cm/s to 5 cm/s. Although, this can be difficult to control unless automated techniques are utilized. In this way, the thickness of the membrane is controlled. With low viscosity solutions, it is sometimes necessary to fill a mold with casting solution rather than cast it (109).

The process used to create hollow fiber membranes is commonly referred to as spinning. The spinning process involves extruding a casting solution through an annular spinneret while a bore fluid flows through the annular center of the apparatus. The flow rate of casting solution and bore fluid are important parameters to consider and are typically set between 0.1 and 0.6 ml/min. Several additional factors influence membrane morphology including the viscosity of the casting solution, the bore fluid properties, as well as spinning parameters (110).

Using either casting or spinning, most single layer membranes can be fabricated. Similar techniques are used to create two layer membranes, but with special instrumentation. For example, a co-casting knife can be used to create two-layer flat sheet membranes with a combination of MMMs and pristine polymer layers (111). Likewise, hollow fiber spinnerets can be equipped with multiple nozzles to create a two-layer hollow fiber membrane (112,113). Both apparatuses are depicted in Figure 4.

4.3 Phase Inversion

Once the casting solution is cast, it is necessary to precipitate the membrane. This can be done using one of three methods: wet, dry, or combination wet/dry phase inversion.

4.3.1 Wet Phase Inversion

Wet phase inversion, sometimes called non-solvent induced phase inversion, can be used for polymer matrices that are insoluble in water or another non-solvent. Once cast, the solution is submerged into an appropriate non-solvent. Demixing of the solvent into the non-solvent occurs rapidly, and the polymer membrane precipitates, typically leaving behind a dense top layer with a porous supporting layer.

It is understood that the kinetics of the demixing process influence the type of porous supporting layer. The demixing process can be explained using a tertiary phase diagram shown in Figure 5 (108).

The binodal line represents the cloud point of the ternary system and is physically the point where demixing begins to occur and the polymer begins to precipitate. The position of the binodal as well as the composition path show interesting trends in terms of membrane morphology. That is, when the so called “instantaneous demixing” occurs, the composition path crosses the binodal line and a finger like structure dominates. When “delayed demixing” occurs, the composition path does not cross the binodal line, resulting in a spongy structure.

The ternary system is strongly influenced by the solvent and non-solvent as the location of the binodal line changes for different components. A typical non-solvent is water since it is inexpensive and environmentally benign, however, other non-solvents such as methanol, hexane, acetone, and xylene have been reported (118,119). The binodal is also strongly influenced by the presence of additives in the casting solution. Water soluble polymers like PEG and PVP, as well as surfactants such as Triton-X, shift the binodal and influence membrane morphology (120,121,122). Interestingly, the presence of fillers also causes a shift in the binodal line. While this phenomenon has not been studied with AC, likely due to the difficulty in visualizing the cloud point in black casting solutions, it was seen with metal particles (117), and likely exhibits similar trends with AC. The shifts in the binodal line are the result of the strong affinity of the non-solvent toward the additives or fillers, preventing the exchange between solvent and non-solvent.

Wet phase inversion usually results in asymmetric membranes with a dense top layer, which is useful in gas phase separation applications. However, by adding pore forming agents or fillers to the casting solution, pores begin to form, creating a membrane suitable for liquid phase separations (99,120).

Adding filler particles to the casting solution tends to reduce the appearance of fingerlike structures and results in spongy cross sections with an ultrathin selective layer as a result of delayed demixing. However, combinations of pore forming agents, surfactants, and fillers can cause interesting morphologies. One example worth noting used a PSF matrix, PEG pore former, and Triton-X-100 non-ionic surfactant. AC was loaded into the MMM with 0.1, 0.5, and 1 wt.% concentrations. The influence of AC loading on MMM morphology was investigated. The use of Triton-X created a fingerlike morphology which broke down with the addition of 1 wt.% AC. The surface pore size also increased with AC loading as shown in Figure 6 (121).

One interesting phenomena that has been documented during wet phase inversion with hydrophobic AC is the tendency of AC to settle near the top surface of the membrane depicted in Figure 7 (91,123). In this case, hydrophobic particles accumulate near the top of the membrane due to the instantaneous exchange of solvent with water at the top of the membrane, resulting in repulsion between AC and non-solvent near the bottom of the membrane causing migration of the AC to the top surface (13,91,123). Thus, increasing the exchange rate between solvent and non-solvent prevents this migration and particles remain randomly embedded.

4.3.2 Dry Phase Inversion

Another method of precipitating the membrane out of solution is by dry phase inversion, often called precipitation by solvent evaporation. In this method, the solvent is removed from the casting solution by evaporation rather than liquid-liquid demixing. The rate of evaporation, and thus the environment, temperature, and pressure, are key variables that influence the membrane properties. Dry phase inversion is typically performed in a vacuum or inert environment at elevated temperatures (15,124). Although, some research has been performed in humid environments where the relative humidity greater than 90% (125). Ambient environments are also utilized where the presence of oxygen and normal humidity levels of less than 60% are considered (90,92). High

humidity levels tend to create areas of nonsolvent induced inversion, creating a slightly more porous surface which greatly influences performance (125). Otherwise, this method tends to produce dense membranes with a nanoporous surface and a dense cross section (126). Increasing amounts of AC produce cross sections with less homogeneity as shown in Figure 8 (89).

One major advantage to the dry phase inversion technique is the thermal treatment of the membrane to influence free volume and chain rigidity (127). Moreover, the addition of AC tends also to influence free volume and chain rigidity mainly due to the AC porosity and crosslinking ability (95). When precipitated under appropriate conditions, this method works complimentary with AC addition.

4.3.3 Dry/Wet Phase Inversion

The final method is a combination of the previous two methods. Typically, solvent in the casting solution is allowed some time to evaporate before being submerged in a non-solvent (10,128,129). The dry phase step is allowed to occur for seconds to minutes, then wet phase inversion completes the precipitation. It is important to note, if complete precipitation occurs during the dry phase step, the effects of the wet phase step are not evident. Hence, the dry phase step should be carefully controlled as to not allow complete solvent evaporation.

In this case, a variety of membrane structures can form. Frequently, the benefits of both methods are evident, creating asymmetric membranes with few surface defects (130). The dry/wet phase inversion method is typically followed for fabricating hollow fiber membranes.

5. Relationship Between Surface Chemistry and Permeability

One of the main advantages of using MMMs is the fillers' influence on the surface chemistry and separation properties of the membrane materials. The use of AC in MMMs has a significant impact on the surface properties of MMMs. Their influence is greatly dictated by AC synthesis conditions such as the temperature of carbonization, temperature of activation and activating agents (131). Consequently, utilizing AC in MMM synthesis has an impact on some surface properties such as wettability, hydrophilicity, hydrophobicity, porosity, surface roughness, polarity and surface charge.

Wettability is a surface property that describes the ability of interaction between a solid and liquid phase, and it is greatly affected by the hydrophilicity and hydrophobicity of the solid phase (2). Wettability can be determined using the surface tension values obtained by measuring the contact angle between the solid phase (the membrane) and the droplet of liquid on the surface. Hydrophilic surfaces tend to have high surface tension values and they are characterized by the existence of active functional groups that have the ability to form bonds with the fluid (2). On the other hand, hydrophobic surfaces have a tendency to have low surface tension values and are characterized by the lack of the active groups. As the contact angle decreases, the surface tension increases which leads to a more hydrophilic membrane (2). On the contrary, increasing the contact angle decreases the surface tension and hence results in a more hydrophobic membrane.

It is important to note that the hydrophilicity and hydrophobicity of AC, as well as additives, in a casting solution are the main factors that govern the wettability of a membrane. The introduction of hydrophilic AC tends to create more hydrophilic surfaces (122), whereas hydrophobic AC results in more hydrophobic surfaces (95). This is dictated by the functional groups present in the AC and their electrostatic interaction with the polymer matrix. Localized electrostatic interactions can cause a shift in electron distribution, creating a more or less polar surface (132). Another possible mechanism to this trend is the migration of AC to the surface, and ultimate rupture, can leave the AC surface exposed (123). The exposure results in high degrees of contact between working fluid and the AC. Thus, the wettability of the MMM surface is defined by the wettability of the AC. Furthermore, the use of surfactants in the casting solution has shown to be the dominant factor, preventing shifts in contact angle regardless of AC loading, as demonstrated by Aghili et al. (121). This is likely due to the smoothing effects of surfactants, leaving behind a smooth surface, while preventing surface migration of AC, balancing any influence of AC (133,134).

Porosity is a surface physical property indicative of the void fraction in a material or on a materials surface. As the amount of AC increases in a synthesized MMM, the membrane becomes more porous which results in a higher flux (120,122). This effect can be potentially attributed to the fact that AC can locally break surface tension, which results in the creation of surface pores in its vicinity. By increasing the frequency of this phenomena through increasing the loading of AC, porosity can be greatly increased (121). This property could be beneficial in the separation of solutes from liquids due to increased wettability and pores available for liquid penetration. In gas separation, on the other hand, porosity if most closely resembled by the FFV, in which gas permeability is highly dependent. AC inherently adds FFV within the membrane due to the highly porous nature of AC. The particles tend to increase the gaps between entangled polymer chains, providing more space for diffusive transport. AC also tends to adsorb high affinity gases. This results in higher rates of diffusion and solubility, hence improved permeation, as was demonstrated by the study by Weigelt et al. (10).

Surface roughness is another physical property that is a function of the surface texture. Generally, there is a directly proportional relationship between the amount of AC loaded and the surface roughness. This typically results in higher fluxes as a result of increased specific area. This increase in surface roughness is attributed to higher surface pore density and uneven settling in the polymer phase caused by the presence of AC and particle agglomeration (121). AC with higher surface area can cause rougher surfaces compared to AC with lower surface area as was shown by Anson et al. (15) and Marchese et al. (124). This is a result of solvent being removed from the pores of AC rather than the polymer. However, surface roughness is usually associated with fouling, an undesirable property that can be mitigated by use of additives. For instance, according to Hwang et al., the addition of PEG to AC-PPSU membranes resulted in lower surface roughness. In membranes with 0.25% AC, the surface roughness was 360.0 without PEG, 72.1 with 6% PEG, and 119.0 with 12% PEG (120).

Polarity is a significant property in membrane science for gas separation. It can be described as an uneven distribution of charge across a molecule where it is believe to govern the gas solubility and

the membrane selectivity (131). For instance, the polarity of a surface tends to increase due to the presence of oxygen complexes on the surface of AC, which impacts the sorption properties of the surface (131). In order for a gas to permeate, the polarity of both the membrane and the gas should match. This means that MMMs with AC tend to permeate more polarizable gases or vice versa depending on the polarity of AC-MMM.

Surface charge generally originates from the dissociation of ionizable groups present at the surface (2). For example, small anions are negatively charged because they are more polarizable than cations and tend to adsorb on hydrophobic surfaces (2). Moreover, surface charge and electric potential are both pH dependent where they shift from negative to positive as the pH decreases from basic to acidic (2). The surface charge is an important property in membrane characterization because it usually correlates to the tendency of fouling or even the state of fouling on membranes (2). Therefore, the more positively charged the surface is, the higher the fouling is in the membrane.

6. Application of AC-MMMs

Various separation applications have been investigated with AC-MMMs. Table 5 summarizes the most relevant recent studies, in terms of the membrane matrix, AC material, and the intended application. Significant findings are highlighted and detailed in following sections.

6.1 AC-MMM uses in Water Purification

6.1.1 Rejection of Heavy Metal Ions

Due to the excellent adsorption capacity of AC, many researchers have investigated AC-MMMs for heavy metal ion rejection. In doing so, the selectivity of the matrix material, as well as the adsorption of the AC, are exploited to result in typically better rejection and permeation compared to the neat membrane or AC alone.

Jinsong et. al., reported 93.7-100% rejection of Cu^{2+} and 95.2-100% rejection of Pb^{2+} with a flux of near 33 LMH using a PSF hollow fiber membrane loaded with biochar (3-50 microns from sugarcane bagasse) (122). They also reported a recovery rate of 140 Lm^{-2} of water from Cu^{2+} solution and 1500 Lm^{-2} from Pb^{2+} solution before the defined breakthrough point (122). In another study by Hosseini et. al., PEI matrix with nano size AC were tested for copper and sulfate ion rejection; where membranes with 0.5 wt.% AC rejected copper ions at 96% and sulfate ions at 94% (123). Both studies observed an increase in flux compared to the pristine membranes with acceptable rejection of both Cu^{2+}, Pb^{2+}, and sulfate; completely attributed to adsorption onto the AC fillers. A different study by Hofman et al. detected differences between using biochar and AC from coal using a PES matrix due to acid functional groups in the AC (136). Biochar was more effective in removing Cu^{2+} at initial concentrations below 10 mg/L, and the AC loaded membrane was more effective with initial concentrations greater than 15 mg/L (136).

PSF loaded with AC from palm kernel shells showed a permeability/rejection tradeoff for Ag^{+}, Pb^{2+}, Cd^{2+}, and Cr^{3+}. Pristine PSF membranes showed low flux, but near 100% rejection of all ions. Flux increased from about 10 LMH to 50 LMH as AC loading was increased from 0% to

0.9%, but major decrements in rejection for all species were observed (135). The optimal AC loading was suggested to be 0.3 wt.% in which rejection followed the order: $Cd^{2+}>Cr^{3+}>Ag^{+}>Pb^{2}$. This is nearly consistent with the order of ionic radii, which would indicate size exclusion rejection. However, Cd^{2+} has the smallest ionic radius but had the highest rejection. This is likely because it could easily penetrate the matrix, but was chemisorbed by the AC. This along with higher rejection with increasing AC loading indicated that size exclusion and adsorption played an important role in the rejection of each ion (135).

With adsorption being the principal mechanism of heavy metal ion rejection, regeneration of the AC within the membrane becomes an issue. Chemical regeneration is required to remove metal ions from AC, but the matrix material must also be considered to prevent damage. He et al. showed that regenerating spent AC-MMMs with nitric acid resulted in acceptable performance, observing a decrease in rejection of Cu^{2+} from 93% to 87% and of Pb^{2+} from 95% to 86% after regeneration (122). Nevertheless, more studies are clearly still needed to better resolve the regeneration issue and comfortably proclaim that the hurdle has been cleared.

6.1.2 Rejection of Uranium

While some conventional separation methods to remove U from water (absorption, ion exchange, precipitation) can be used, they typically only have high rejection when treating solutions with high U concentrations (on the order of ppm) (137,145). However, U typically exists in relatively low concentration in water (on the order of ppb), making it difficult to remove using these methods. MMMs have been demonstrated to capture U from water at these lower concentrations via a combination of size exclusion and adsorption.

Rodriguez et al. investigated a CTA membrane with micron sized commercial AC for dilute (0.7 ppm) U removal (4). Membranes with 3 wt.% AC loading achieved the highest U removal of 41% with a feed pH of 7. The flux across the membranes averaged 363 LMH/bar. The high flux and high rejection, despite agglomerates and apparent pH rejection dependence, indicate adsorption of U on the AC was the predominant mechanism of separation.

The same group was able to increase the U removal of dilute solutions to 50% by introducing iron into the uranyl feed solution or by incorporating iron into the AC by chemical impregnation (138). This effect also indicated that adsorption dominated rejection. Additionally, in using the MMM with iron doped AC, homogeneous dispersions of AC were achieved, which allowed for more efficient adsorption. Although adsorption appeared dominant, the group noted complex rejection behavior for various species in the uranyl solution with varying pH, indicating size exclusion was also present.

6.1.3 Rejection of Aromatic Compounds

Phenol is a high priority water pollutant that is commonly studied (146). The removal of phenol from water can be achieved with both ultrafiltration and adsorption using MMMs, making them an ideal class of membrane for this process.

Saranya et al. used a PPSU matrix with functionalized AC from *acacia fumosa* seeds for the removal of phenol from water (99). Functionalizing the AC aimed to prevent agglomerations in the casting solution and ultimately within the membrane and to increase rigidity to maintain active sites for adsorption. The pristine polymer had nano-sized surface pores when cast and precipitated by wet phase inversion, as has been documented before (147,148). The surface pore size increased to nearly one micron until the surface became dense with 1% loading of AC. This indicated that even with functionalized AC, agglomerations still formed at high loadings and pore blockage by AC become more apparent.

The phenol rejection efficiency by the MMMs was found to increase with AC loading. However, the amount of phenol adsorbed by the AC decreased with higher loadings (99). This indicated that active adsorption sites became less available, marking a shift between adsorption dominated rejection to a combination of adsorption and size exclusion. The flux first increased from 14.5 LMH in the pristine polymer to 26.9 LMH in the 0.25 wt.% functionalized AC loading and then decreased as the loading increased to 1 wt.% as a direct result of decreased porosity and fewer surface pores.

The use of nano sized (750 nm) AC seemed to prevent agglomeration in a CAP membrane, allowing for 25 wt.% loading (91). A flux of 64 LMH flux and 96% rejection for phenol was attributed to an increase in both specific surface area and hydrophilicity compared to the pristine membrane due to the AC. These two properties appeared to maximize the flux and active sites available for adsorption as depicted in Figure 10. Despite the high concentration of AC near the membrane surface, fouling was still present and 10% reduction in flux was seen even after acid-alkali regeneration, indicating irreversible fouling (91).

The same group also investigated a 70 nm AC in a hollow fiber PSF matrix (13). Although surface pores were visible in the pristine and low loaded membranes, they noted a decrease in surface pore volume at AC loadings larger than 1 wt.% as a result of pore blockage (13). As noted before, the addition of AC lead to a more hydrophilic membrane, however, the PWF decreased with increasing AC loading. This signifies competition between pore blocking and surface hydrophilicity on flux. In this case, the pore blockage was more dominant, restricting flux.

They also found that a membrane with 2 wt.% AC was optimal in terms of flux and adsorption of benzene, toluene, and phenol. The pH dependent rejection was attributed solely to adsorption by the AC, and was a maximum of 96% for benzene, 88% for toluene, and 80% for phenol at a pH of 4 (13). The influence of pH was shown to influence the zeta potential of the MMM surface. Acidic solutions resulted in higher zeta potentials. Thus, less polar molecules could more easily be adsorbed by the AC in the MMM. Hence, the lower rejection for phenol was primarily caused by its negative -OH functional group, limiting its adsorption. The $–CH_3$ group on toluene is slightly less negative, promoting higher adsorption than phenol. The absence of negative functional groups on benzene was the reason for its high adsorption.

Another aromatic water pollutant that has been investigated by AC-MMMs is humic acid. The rejection of humic acid is commonly probed in membrane applications because it is a major source of fouling on many polymeric membrane materials (16,149,150). A study by Lin-Luen et al. used a PEI-PPSU polymer blend, which was loaded with 0.25wt.% AC from bamboo and 6 wt.% PEG as a pore forming agent, to achieve a removal efficiency of 84%, as shown in Figure 11 (120). The addition of PEG not only helped create a spongy cross section with surface pores, but additionally helped in reducing surface roughness caused by the addition of AC. In membranes with 0.25 wt.% AC, the surface roughness was 360.0 without PEG, 72.1 with 6 wt.% PEG, and 119.0 with 12 wt.% PEG (120). This is an interesting observation since rougher membranes typically lead to higher degrees of fouling. Hence, adding PEG can potentially mitigate fouling. Membrane porosity was also improved by the addition of AC as measured by PWF. As the AC loading increased from 0.25 wt.% to 1 wt.% without the addition of PEG, the PWF increased from 271 to 535 LMH (120). The exception was in membranes with 0.50 wt.% AC, adding 12 wt.% PEG into the casting solution slightly increased the PWF from 428 to 452 LMH (120).

6.2 AC-MMM uses in Biological Solute Rejection

The separation of biomacromolecules from various media pose an interesting challenge for membrane processes, mainly due to fouling issues. Some researchers have investigated AC-MMMs for biological solute rejection, utilizing their antifouling properties and enhanced permeability resulting from pore formation.

6.2.1 Removal of Organic Matter

PSF matrix loaded and coated with powdered AC (<74 microns from sorghum) proved to be effective for the removal of organic matter from cheese whey wastewater (121). The rejection was quantified in terms of COD and UV_{254}.

AC-loaded membranes showed improved rejection of COD and UV_{254} shown in Figure 12a. The COD rejection increased from 38% in neat membranes to 44% in 0.5 wt.% AC-MMMs. Similarly, UV_{254} removal increased from 42% to 48%. A rejection decline in both was seen with 1 wt.% AC-MMMs. The waste water flux, shown in Figure 12b, was similar in membranes loaded with 0.1 and 0.5 wt.% AC, and was higher than both the neat membrane and the membrane loaded with 1 wt.% AC (121). Though, all membranes showed a decline in flux with time, indicating pore blockage and cake formation on the membranes.

To combat cake formation, AC was used to coat the 0.5% loaded membrane. When coated with 30 g/m^2 AC, rejection increased to about 80% due to the additional sites for adsorption. In membranes coated with more than 30 g/m^2, there was no increase in rejection due to AC agglomeration leading to fewer active sites (121). Surprisingly, the waste water flux increased proportional to the amount of coating despite the extra thickness caused by the added layer. The coated membranes still showed a flux decline with time, indicating fouling was still present. However, after physically cleaning the surface, the waste water flux returned to near its original value before filtration. As shown in Figure 12, the flux of the coated membrane remained constant

after cleaning, whereas the neat and uncoated membranes saw a flux decline after cleaning. This means the irreversible fouling was reduced by coating the MMMs with AC.

6.2.2 *E. Coli.* Removal

Considering *E. coli.* is relatively large (0.5 microns wide by 2 microns long) and leaves membranes susceptible to bacterial growth over time, antimicrobial membranes with relatively large pores can be advantageous.

Hassan et al. investigated a novel MMM configuration made with two layers for the removal of *E. coli.* (78). It consisted of oxidized CNF intertwined with AC deposited on a porous paper support covered in un-oxidized CNF and a PAE crosslinking agent. Two methods of formation were investigated. 1) direct drying and 2) rinsing with isopropyl alcohol prior to drying. Drying with isopropyl alcohol resulted in membranes with a more porous surface (78). The membrane with AC in the bottom layer was more porous than membranes without the AC in the bottom layer.

In the membranes formed by direct drying, adding the AC layer enhanced PWF, from 55 LMH without AC to 158 LMH with AC, due to pore formation in the CNF layer even though the AC was not directly introduced into that layer. Increased PWF was observed with the isopropyl alcohol drying, and the membrane with AC showed relatively higher PWF as they saw an increase from 165 LMH to 425 LMH as a result of the AC. The flux with bacteria suspensions was significantly lower, at 139 in CNF and 345 in CNF-AC, which was a result of pore blockage by the bacteria (78). The removal of *E. coli.* was slightly improved from 97% to 99% with the addition of AC, as a result of adsorption by the AC layer. They found that the CNF-AC membranes were antibacterial, showing no growth after 24 hrs. at 37°C (78).

6.2.3 Blood Plasma Toxin Removal

In purifying blood plasma, it is crucial to prevent contamination, thus AC presents some hazards as AC-MMMs pose the risk of particles breaking free and entering the passing fluids (151). One method to ensure this does not happen is by using a two-layer membrane with a pristine polymer on one side.

A two-layer PES-PES/AC membrane was investigated for the removal of creatinine from blood plasma by Tijink et. al. and is shown in Figure 13(a) (111). The particle free PES layer was used to ensure AC was not mixed with the retentate. This two-layer architecture was achieved using an adjustable co-casting knife. The cross sections were influenced by a PVP additive in the casting solution, and 60% NMP in the coagulation bath for the phase inversion. They showed that between 50-70% AC relative to the PES could be loaded while maintaining a spongy cross section (111). This architecture observed decreased water permeance from 1839 LMH/bar in the single layer MMM to 350.7 LMH/bar in the dual layer. This is likely a result of the surface of the particle free layer adding resistance to flow. The particle free layer did not reduce creatinine concentrations, whereas the single layer MMM and dual layer particle free-MMM reduced concentrations by about 80% (111). This was compared to creatinine adsorption on the AC alone, and was similar, indicating that the active sites on the AC in the MMMs were readily accessible (111). Both diffusion of creatinine through the membrane as well as adsorption by the AC was simultaneously

responsible for the removal of creatinine (111). It is important to note that this removal was accomplished without major changes in plasma osmolality, pH, or total protein concentration. Major changes in these values would be detrimental to dialysis patients.

Tijink et al. also studied the removal of other toxins from plasma with a two layer hollow fiber membrane depicted in Figure 13(b) (112). This configuration was achieved using a triple layer spinneret. PES/PVP/AC membranes were fabricated by the dry-wet spinning method in air and further precipitated in PVP or NMP solutions. They observed good dispersion of AC with no macro void formation. Using a 5% PVP in water solution as the bore fluid resulted in a circular bore, whereas using only water resulted in irregular shapes (112). The membrane with the highest pure water permeance was made with the NMP containing bore fluid and was used throughout the study. The clean water permeance was 58.4 LMH/bar and it was shown that no delamination or AC losses occurred.

Creatinine was investigated as the water soluble toxin. HA, IS, and PCS were also investigated and represented PBTs (112). The creatinine adsorption by the hollow fiber membrane of 100 mg/g was higher than the flat sheet configuration at 29 mg/g for the same feed concentration. Creatinine, HA, IS, and PCS all showed similar adsorption capacities in the dual layer MMM as was also observed in the AC alone, indicating good accessibility. In cross flow measurements, nearly 40 mg/g (creatinine/membrane) was removed after 4 hours. The removal of PBTs in cross flow was mostly attributed to adsorption on the MMM. This is in contrary to creatinine rejection, which combines adsorption with diffusional effects. Removal, in mg PBT per gram of membrane, was about 14 for HA, 3.5 for IS, and 2.3 for PCS (112). It is important to note that albumin was able to pass through the membrane and osmolality decreased over time. However, no changes in pH or salt concentrations were detected.

6.3 AC-MMM uses in Pervaporation

Pervaporation has frequently been investigated for the dehydration of organic compounds, especially alcohols. This process offers a unique cross between liquid and gas phase separation because both phases are in contact with the membrane. Thus, the rejection of a polar liquid species on the surface and the diffusion of a less polar gaseous species in the free volume of a membrane is required. This provides an interesting challenge for AC-MMMs due to the AC influence on surface hydrophobicity and free volume. Moreover, as most AC-MMMs result in hydrophilic surfaces, modifications to the AC are required for enhanced properties.

Lan et al. investigated the modification of biochar created from lodgepole pine bark with KH-550 and YDH-171 (95). The nano-sized “grafted biochar” was loaded into a PDMS membrane and cast on a cellulose acetate support and allowed to precipitate in air for 24h. The grafting resulted in weaker –OH stretches in the biochar, and ultimately an increase in water contact angle and a decrease in ethanol contact angle in the MMMs. These changes indicated that the neat membranes became more hydrophobic with the addition of grafted biochar and has a stronger affinity toward ethanol (95). The hydrophilicity on the YDH-171 was stronger than KH-550 due to the presence

of a hydrophilic -NH_2 in KH-550. Likewise, MMMs with YDH-171 showed stronger compatibility with ethanol.

Both biochars showed an increase in flux with an increase in loading up to 4 wt.% due to an increased free volume. However, the separation factor decreased in both cases after 3 wt.% likely due to the formation of macrovoids within the membrane. An increase of ethanol in the feed solution resulted in lower flux but higher separation factors. MMMs loaded with 3 wt.% biochar at 40°C and 10 wt.% ethanol feed concentration performed best. The YDH-171 MMM performed relatively better with a separation factor and flux of 11.3 and 227 LMH. The KH-550 MMM had a 10.1 separation factor and a flux of 225 LMH (95).

Another AC that resulted in MMMs with stronger affinity toward the alcohol was nano sized (20-40nm) AC with higher specific surface area (1400 m^2/g) (109). When fabricated by the dry phase inversion method, the addition of AC resulted in a rougher PDMS surface, increased degree of swelling, and an increase in water and butanol contact angle caused by the AC (109). A lower contact angle was seen with butanol than water, indicating higher affinity of butanol with the membranes. The permeability of both butanol and water increased when AC loading was increased from 0 to 6%, but then decreased slightly at 8% loading. However, the separation factor increased for the entire range of AC loadings (109). The decrease in permeability from 6 to 8% loadings was likely the result of agglomeration forming within the membrane, creating a longer path for diffusion. Optimal results were seen at 6% AC loading with a butanol permeability of $9.49x10^{-7}$ g cm/s cm^2 bar. Separation factor increased with increasing temperatures within the range of 37-57°C.

6.4 AC-MMM uses in Gas Separation

The use of MMMs has especially attracted attention for gas phase separations due to the permeability/selectivity limitations of polymeric and inorganic membranes. MMMs offer multiple mechanistic pathways (152) capable of exceeding the permeability and selectivity upper bounds suggested by Robeson (153). Moreover, Chuah et al. recently formulated a metric for MMM performance based on filler/matrix properties (154). They presented an "F-index" which quantifies improvements in permeability and selectivity. AC and CMS MMMs consistently showed F-index values greater than 1 with many polymers, meaning they are likely to improve both permeability and selectivity in MMMs.

Although Robeson's upperbounds were correlated specifically for membranes undergoing solution diffusion, AC-MMMs are often compared to this upperbound (10). However, the use of this comparison may not be accurate not only because of the mechanistic difference, but also because of the difficulty in establishing and measuring the active layer used in the permeability calculation. Nonetheless, AC-MMMs have shown promising results for two classes of gasses: small, low molecular weight, non-polar gas mixtures and higher hydrocarbons.

6.4.1 Small, Low Molecular Weight, Non-Polar Binary Mixtures

The gas pairs consisting of a combination of He, H_2, O_2, N_2, CO_2, CH_4 present some of the most difficult, industrially relevant gases to separate due to their similar size, polarity, and low boiling

points. The use of AC-MMMs has yet to be exceptionally successful in their separation, however, many important studies offer insight into their behavior.

The influence of AC size was investigated in an ABS copolymer membrane for CO_2/CH_4 separation (15). Two AC of different particle size were utilized. The AC with lower surface area and larger size ultimately lead to better CO_2/CH_4 permselectivity. However, more filler was needed to achieve this. It was suggested that poor polymer filler interaction was improved by the butadiene-styrene block in the matrix. Both CO_2 permeability and CO_2/CH_4 selectivity was improved with the addition of AC particles. Higher loadings led to further increases in permselectivity up to 10 wt.% in the smaller AC, and 40 wt.% in the larger AC (15). Increases in permeability and selectivity were attributed to selective surface diffusion through the pores of the AC. This is reasonable considering CO_2 is the more adsorbable of the two species. The use of dry phase inversion technique was critical to the increase in permeability, as nano-sized pores and surface roughness were enhanced with the addition of AC (15,124). Moreover, AC with higher surface area and pore volume resulted in increased roughness due to the solvent being eliminated from pores in the AC rather than from the polymer (124). This results in localized variation in mass transfer around the AC particles, creating a higher tendency for node and valley formation compared to pristine membranes (155).

The influence of particle surface area was opposite to this finding in a Matrimid-CMS MMM. Two different CMS nanoparticles (1079 and 538 m^2/g BET) showed similar performance when used for CO_2/N_2 separation (11). In this case, the gas diffusion through the particle/matrix void space was more significant than the diffusion through the particle pores. None the less, membranes showed improved performance compared to pristine Matrimid, with a 14.9 barrer permeability and 38.9 ideal CO_2/N_2 selectivity (11).

On the other hand, a PEBAX matrix loaded with 25 and 50 wt.% (relative to the polymer phase) AC saw a different trend (139). Similar CO_2/CH_4 selectivity was seen in the neat and 25 wt.% loaded membranes, but a large drop in selectivity was observed at 50 wt.% loading. CO_2 permeance was the following order: neat PEBAX<25%<50%. The increase in permeability was attributed to diffusion through the pores of the AC as well as unselective void space in the 50 wt.% loaded membrane (139). This is further evidence that there is an optimal loading before the formation of unselective void space.

Garcia at el. also studied AC loaded in a PEI matrix (90). Using optical microscopy, they were able to determine that 2% loading of AC resulted in homogeneous dispersion of AC in the PEI. At higher loadings, agglomerations were observed by measuring visible particle size and comparing it to the original particle size distribution. (90). It was also shown that the d-spacing decreased with increasing AC loadings, likely the result of rigidification of the polymer structure. They also saw an increase in pure gas permeability in all pure gases tested with increased AC loading. A simultaneous increase in selectivity for H_2/CH_4, H_2/CO_2, and O_2/N_2 gas pairs was also observed, resulting from a decrease in the diffusion coefficient and an increase in solubility due to preferential sorption of O_2, CO_2, and CH_4 in the AC particles (90).

The same group studied a PVC membrane cross-linked with a difunctional amine: 4,4'-oxidianiline loaded with AC up to 60 wt.% (102). After creating the casting solution, AC agglomerations were filtered. They noted that the top and bottom surface of membranes loaded with 60% AC were similar and contained visible void spaces around the AC (102). Using a crosslinking agent favored the formation of a less permeable porous structure. X-ray diffraction revealed that cross linked membranes had a lower degree of crystallinity aided by AC loading. Thermogravimetric analysis showed that as the AC content reached 60 wt.%, the thermal behavior was dominated by AC rather than matrix phase. Increasing amounts of cross linking and AC loading also influenced an increase in gas permeability as predicted due to void spaces in the membrane surface (102). Membranes loaded with 60% AC showed Knudsen selectivity as a result of that void formation. However, their selectivity was dissimilar to the Knudsen selectivity in cross-linked membranes with 23 wt.% AC. They suggested a combination of sorption-diffusion and Knudsen diffusion was observed (102).

Another study demonstrated that a reduction in surface defects was shown to occur by using a dry/wet phase inversion method on an AC loaded Matrimid matrix (10). Solvent and non-solvent were chloroform and methanol. Good polymer-AC interaction was verified by an increase in glass transition temperature with an increase in AC loading (10). Despite the AC causing a rougher surface than pristine membranes, the AC tended to accumulate near the bottom of the membrane due to settling during the dry phase inversion step.

For all gases, there was an increase in permeability with increased AC loading and very small changes in selectivity for most gas pairs. A significant difference between the measured selectivity and the predicted Knudsen selectivity showed that solution diffusion was the primary mechanism, attributing the increase in permeability as a result of adsorption and surface diffusion through the AC (10).

The formation of void spaces with high amounts of AC was also apparent in a PES matrix. With 10 wt.% AC, macrovoid formation was present as a result of poor compatibility (92). The O_2 and N_2 permeance was higher in the MMMs than pure PES, showing increased transport proportional to increased AC loading until 10%. A similar trend was seen in O_2/N_2 selectivity, where an increase in selectivity was observed with membranes made with 1 and 5 wt.% AC followed by a decrease at 10 wt.%. Still, this decreased selectivity was higher than the pure PES (92).

Vu et al. showed that priming of CMS with small amounts of PSF before being placed in contact with dissolved Matrimid helped to decrease agglomeration and interfacial defects (7). Moreover, thermal annealing in combination with priming significantly reduced defects, enabling defect free membranes at loadings of 35 vol.%. Interestingly, this led to an increase in selectivity for CO_2/CH_4 and O_2/N_2 but overall lower permeabilities than the pristine polymer.

Facilitated transport of CO_2 by alkanolamine embedded in dense PES-CMS membranes proved to be highly effective for CO_2/CH_4 separation (81,140). In this case, CMS and the alkanolamine components opened multiple pathways for gas transport through the membrane. Increased loading of the alkanolamine solution resulting in increases in CO_2 permeance while maintaining CH_4

permeance. This resulted in a CO_2 permeance of 117.32 GPU and CO_2/CH_4 selectivity of 20.1 with a membrane made of 20 wt.% PES, 30 wt.% CMS, and 15 wt.% alkanolamine in NMP (81,140).

When compared to MMMs containing other common fillers, CMS and AC-MMMs perform average in the case of CO_2/N_2 and H_2/CH_4 separation. In the case of CO_2/CH_4, O_2/N_2, and H_2/CO_2, several of these membranes showed superior performance. This comparison is shown in Figure 14, where various MMMs were grouped by filler type. Plots were constructed from data listed in various review articles (17,18,20,21,24,82,94,152,156) as well as other recent literature. While the choice of matrix material is of crucial importance, these plots demonstrate the viability of using AC in MMMs. They also highlight the need for more studies, as there is no apparent trend seen in AC-MMMs for these applications.

6.4.2 Higher Hydrocarbons

The separation of higher hydrocarbons (C3+) from methane is also a challenging task is which membranes can compete with existing technologies (157).

Mushardt et al. studied a POMS MMM loaded with AC at 1.5 and 3.5 microns particle size for the separation of n-C_4H_{10} and CH_4 (89). A silicon coating was applied to seal surface defects. Adsorption studies on the AC particles showed that the AC had a higher affinity toward n-C_4H_{10} than CH_4. As the amount of AC loading increased, membrane cross sections became less homogeneous and were more pronounced for smaller AC sizes. Defects were seen with 40 wt.% (relative to polymer) loaded membranes despite silicon coating. Smaller particles tended to result in more frequent defects (89).

That same study also found that the addition of AC led to a reduction in the swelling effect commonly caused by n-C_4H_{10} and a decrease in n-C_4H_{10} permeance proportional to increased AC loading. MMMs with smaller particles showed higher permeance compared to the larger particles. However, membranes with 20 wt.% (relative to polymer) loading showed the highest n-C_4H_{10}/CH_4 selectivity. They concluded that particle size had little influence on selectivity, indicating that pore size, not particle size, controlled permselectivity behavior in these membranes (89).

A follow-up from the same group studied the performance properties of mixed gases of higher hydrocarbons using the same POMS-AC MMM (79). They noted that swelling caused by n-C_4H_{10} uptake played an important role in both permeability and selectivity. Using a mixture of 5 mol% n-C_4H_{10} in CH_4, they saw higher n-C_4H_{10} permeance in the pure POMS membrane, but a higher selectivity in the MMM containing 20 wt.% AC. For feeds with less than 2% n-C_4H_{10}, the permeance of n-C_4H_{10} was lower in the MMMs, and the selectivity was equal for both membranes (79).

They also tested a gas containing 19% of higher hydrocarbons consisting of CH_4, CO_2, C_2H_6, C_3H_8, n-C_4H_{10}, and $_n$-C_5H_{12}. The permeance of each species followed the condensability, increasing proportionally with the number of carbons. Likewise, selectivity with respect to CH_4 also increased with number of carbons (79).

6.5 Proton Exchange AC-MMMs for a Direct Methanol Fuel Cell

Important parameters in proton exchange membranes for a direct methanol fuel cell are proton conductivity, limited methanol permeability, and overall stability. AC-MMMs contend for this application because the polymer serves to provide flexibility and ion exchange capacity while the AC serves to enhance dimensional, thermal, and mechanical stability and enhance proton conductivity and water uptake (158).

Nafion is the most common membrane material for fuel cell applications. It is typically formed by tradition phase inversion or sol gel methods. AC can be introduced into the casting solution readily before inversion (142,143). Chai et al. utilized a unique method to produce and incorporate AC into a Nafion in a single step. A glucose solution was introduced to a swollen membrane and then hydrothermally reacted to carbonize the glucose (144).

Hydrophilic AC can be used to improve the water uptake in proton exchange membranes. The increase of water in the membrane enhances proton conductivity, improving the performance of the membrane. Several studies have shown this increase. Guo et al. reported an increase from 28% to 48% water uptake with 1 wt.% nano AC (141). A similar increase was observed by Tsai at al., however 15 wt.% AC was need to achieve 65% water uptake (142). Chai et al. further demonstrated the water uptake potential, measuring 140% uptake with a 10 wt.% AC loading (144). At low loadings, this variation with AC loading is the direct result of hydrophilic properties of the AC. At higher loadings, the AC may become agglomerated, reducing active sites available for water adsorption. In turn, the water uptake becomes limited with increasing AC loading. The increase in water uptake and electrostatic repulsion of AC to methanol resulted in an increase in proton conductivity and simultaneous decrease in methanol permeability (144). Importantly, the power density is also influenced by introducing AC. With 3.6 wt.% AC, an increase from 25.2 $mWcm^{-2}$ in pristine Nafion to 36.3 $mWcm^{-2}$ in one instance (144). However, with AC loading exceeds a certain concentration, increased resistance between the membrane and electrode can occur, resulting in a reduced power density. Likewise, too high loading resulted in particle agglomeration leading to poor mechanical performance, hindering the viability of AC-MMM use.

7. Predictive Models

Modeling is regularly needed and used to guide experiments, design specific unit operations, and optimize process. Because of this, many predictive models have been developed for MMMs. A thorough review of these models was conducted, presenting numerous models for MMMs in ref. (152). However, there are no apparent studies that have aimed to develop models specifically for AC-MMMs. This is likely due to the complexity of pore size distribution, functionality, and irregular shapes of most AC, rendering general predictive behavior difficult to formulate (122). Nonetheless, existing models have shown some accuracy for AC-MMMs and are further discussed.

In liquid phase separation, the rejection of dissolved solutes can be predicted with adsorption isotherms. Several studies have highlighted the similarity between amount adsorbed on standalone AC, and AC-MMMs (4,13,78,122,123)

As AC has traditionally been used as an adsorbent, much research has been performed on isotherm type specifically for heavy metal ions including arsenic (V), cadmium (II), copper (II), mercury, nickel (II), lead (II), magnesium, and zinc (159,160). Typically, a Langmuir isotherm (monolayer coverage) describes the equilibrium adsorption well, although, the Freundlich isotherm (monolayer) is relatively common for high concentration solutions. The Langmuir isotherm also accurately depicts adsorption of larger molecules such as creatinine (112) and phenol (91). It is important to note that these isotherms depict the equilibrium adsorption capacity, making them accurate for cross flow filtration setups with recycled streams. Adsorption kinetics are required to accurately predict rejection with cross flow or dead end filtration systems without recycle streams. Some researchers have found diffusional effects to be slightly influential on predictability, for example with the removal of phenol from water (99) and creatinine from blood plasma (112). The common equilibrium isotherms that help predict liquid separation by AC-MMMs are shown in the following equations:

Langmuir
$$q_e = \frac{Q_m K_a C_e}{1 + K_a C_e} \quad (1)$$

Freundlich
$$q_e = K_F C_e^{1/n_f} \quad (2)$$

Temkin
$$q_e = \frac{RT}{b_T} \ln(K_T C_e) \quad (3)$$

where q_e is the mass normalized equilibrium adsorption amount, Q_m is the maximum adsorption capacity of a solute on AC, C_e is the equilibrium concentration of the permeate, R is the universal gas constant, T is temperature, K_a is the Langmuir constant, K_F and n_f are Freundlich constants, and K_T, is the Temkin constant.

Kinetic isotherms can also be useful for AC-MMMs. With the known AC loading and an estimation of the time constant within the membrane, the permeate concentration can be estimated. Three common kinetic isotherms which have been applied extensively to AC adsorption are shown here in their linearized form:

Pseudo 1st order
$$\log(q_e - q_t) = \log q_e - \left(\frac{k_1}{2.303}\right) t \quad (4)$$

Pseudo 2nd order
$$\frac{t}{q_t} = \left(\frac{1}{k_2}\right) + \left(\frac{1}{q_e}\right) t \quad (5)$$

Intra-particle Diffusion
$$q_t = k_d t^{1/2} \quad (6)$$

Where q_t is the mass normalized amount absorbed at a given time, t. k_1, k_2, and k_d are the rate constants associated with each model.

The study of gas adsorption on AC has also been studied. The adsorption of He, H_2, O_2, N_2, CO, CO_2, and H_2O are typically modeled well by isotherms assuming monolayer coverage, specifically Langmuir and Freundlich isotherms. The adsorption of CO_2 on AC has been the major recent application of study, which is more frequently modeled with the Freundlich isotherm (160).

Although isotherms predict equilibrium concentrations and the adsorption capacity of gases on AC, they are rarely used to predict the behavior of gases in MMMs because diffusional effects have a more pronounced effect on permeability and selectivity, and MMMs are rarely studied in transient states. Thus, the adsorption of gases on the AC plays no part in selectivity once saturated. One-dimension mass transfer in two phase systems can be used to model gas behavior, but a number of simplifications and assumptions must then be made regarding diffusion in both phases as well as in the interface between AC and matrix (89). Other models have been used to predict gases permeability in AC-MMMs including the Maxwell, Bruggeman, and GPG models. Although these models have not shown to be extremely accurate in AC-MMMs, they are simple to solve, and have shown acceptable results when compared to some experimental data.

The Maxwell model, which was originally developed to predict the electric conductivity of composite materials, was adopted for permeability of gases and is accurate for dilute particle loadings up to 20 vol.% (10). The Bruggeman model more accurately predicts the permeability of AC-MMMs with medium particle loadings between 0-40 vol.% (10). The GPG model is a modified form of the Maxwell model and is based on the model of a hard sphere (161). It has been validated for both liquid and gas permeation for AC contents up to 15 vol.% (152,162).

Maxwell
$$\frac{P_{eff}}{P_c} = \frac{P_d + 2P_c - 2\varphi_d(P_c - P_d)}{P_d + 2P_c + \varphi_d(P_c - P_d)} \tag{7}$$

Bruggeman
$$\frac{P_{eff}}{P_c} = \frac{1}{(1-\varphi_d)^3}\left(\frac{\frac{P_{eff}}{P_c} - \frac{P_d}{P_c}}{1 - \frac{P_d}{P_c}}\right)^3 \tag{8}$$

GPG
$$\frac{P_{eff}}{P_c} = 1 + 3\beta\varphi_d + K\varphi_d^2 \tag{9}$$

In these models, P_{eff} is the effective permeability, P_d and P_c are the permeability in the dispersed (AC) and continuous (matrix) phase, φ_d is the volume fraction of AC, and K is a correction factor defined in terms of β:

$$\beta = \frac{P_d - P_c}{P_d + 2P_c} \tag{9a}$$

$$K = a + b\varphi_d^{1.5} \tag{9b}$$

$$a = -0.002254 - 0.123112\,\beta + 2.93656\,\beta^2 + 1.690\;\beta^3 \tag{9c}$$

$$b = 0.0039298 - 0.803494\,\beta - 2.16207\,\beta^2 + 6.48296\;\beta^3 + 5.27196\;\beta^4 \tag{9d}$$

In this case, β is bound by -0.5 ≤ β ≤ 1. For $\varphi_d \ll 1$, the GPG model simplifies to the Maxwell model (152).

Several more complex models have been developed for predicting behavior of MMMs. Although not extensively used to model AC-MMMs, many accurately predict the behavior of CMS-MMMs (8). Major differences between the simple models presented in Equations 7-9 and the more complex models is a consideration for particle shape, maximum particle loading achievable, presence of a permeable layer between particle and matrix, or some combination. These are factors are essential to consider for general models where different fillers can have vastly different properties (163).

The Maxwell-Wagner-Sillar model takes into account the particle shape, estimating it as an ellipsoid (152). This is determined by the variable, n, which is bound $0 < n < 1/3 \;\; and \;\; 1/3 < n < 1$. The model reduces to simple parallel/series resistance based models when n is an extreme. Similarly, the Cussler model estimates the shape as a flake represented by the flake aspect ratio, α_f (152). This model may find particular accuracy with some CMS-MMM due to their potentially high aspect ratio.

Both the Lewis-Nielsen and Pal models include a shape factor, α, which can be used to fit experimental data, or taken as the inverse diameter when particles are modeled as tubes (152). Each also considers a maximum packing volume fraction achievable in MMMs, φ_m. For particles estimated as a sphere, this value is 0.64, but can by any fraction dependent on the particle size distribution, shape, and aggregation tendency. When φ_m approaches 1, the Lewis-Nielsen model reduces to the Maxwell equation and the Pal model reduces to the Bruggeman equation.

The Felske model contains multiple parameters to account for a permeable layer between the particle and matrix (152). This type of filler is otherwise known as a core-shell. The particle is the core surrounded by some permeable shell. To account for permeability in this layer, the permeability of the species of interest in that interface layer, P_I, is required. To account for the thickness of the shell layer, a parameter δ is defined as the ratio of outer diameter shell to outer diameter of the core. This may find use in AC-MMMs where particles are grafted or interfacial polymerization is conducted at the particle/matrix interface.

Maxwell-Wagner-Sillar

$$\frac{P_{eff}}{P_c} = \frac{nP_d + (1-n)P_c - (1-n)\varphi_d(P_c - P_d)}{nP_d + (1-n)P_c + n\varphi_d(P_c - P_d)} \quad (10)$$

Lewis-Nielsen

$$\frac{P_{eff}}{P_c} = \frac{1 + 2\varphi_d(\alpha - 1)/(\alpha + 2)}{1 - \psi\varphi_d(\alpha - 1)/(\alpha + 2)} \quad (11)$$

$$\psi = 1 + \left(\frac{1 - \varphi_m}{\varphi_m^2}\right)\varphi_d \quad (11a)$$

Pal

$$\frac{P_{eff}}{P_c}\left(\frac{\alpha - 1}{\alpha - \left(\frac{P_{eff}}{P_c}\right)}\right) = \left(1 - \frac{\varphi_d}{\varphi_m}\right)^{-\varphi_m} \quad (12)$$

Cussler

$$\frac{P_{eff}}{P_c} = \frac{1}{1 - \varphi_d + \frac{1}{\frac{P_d}{\varphi_d P_c} + 4\frac{1 - \varphi_d}{\alpha_f^2 \varphi_d^2}}} \quad (13)$$

Felske

$$\frac{P_{eff}}{P_c} = \frac{2(1 - \varphi_d) + (1 + 2\varphi_d)\beta/\lambda}{(2 + \varphi_d) + (1 - \varphi_d)\beta/\lambda} \quad (14)$$

$$\beta = (2 + \delta^3)\frac{P_d}{P_c} - 2(1 - \delta^3)\frac{P_I}{P_c} \quad (14a)$$

$$\lambda = (1 + \delta^3) - (1 - \delta^3)\frac{P_d}{P_I} \quad (14b)$$

All models predict an increasing permeability for increasing AC loading when $P_d > P_c$. Considering AC is highly porous, this is a reasonable prediction and as such, an example of this situation is depicted in Figure 15. .

When comparing experimental data to the models presented, three known variables are necessary, P_d, P_c, and φ_d. There are a number of methods to measure P_d and P_c, including constant pressure-variable volume apparatuses, or constant volume-variable pressure apparatuses. Similar techniques can be used to determine P_I for use in the Felske model. Time lag measurements can also be taken to determine the diffusivity coefficient. Using pure continuous phase adsorption measurements and Henry's law, the solubility coefficient can be calculated. Multiplying the two coefficients, the permeability can be calculated.

While the volume fraction of AC is defined in the formation of the casting solution, slight variances can occur between forming the casting solution and casting. For a better estimation of φ_d , Weigelt et al. (10) suggested using thermogravimetry by first finding the weight fraction of AC, w_{AC}, using,

$$w_{AC} = \frac{m_{MMM} - m_{matrix}}{m_{AC} - m_{matrix}} \tag{15}$$

where m_{MMM}, m_{matrix}, and m_{AC} are the final mass of the MMM, matrix, and AC after degradation under inert conditions at 1000°C. The volume fraction of AC is then calculated based on the density of each component ρ:

$$\varphi_d = \frac{1}{1 + \left(\frac{\rho_{AC}}{\rho_{matrix}}\right) * \left(\frac{1}{w_{AC}} - 1\right)} \tag{16}$$

8. Suggestions for Future Work

Although AC shows promise as a filler in MMMs, several fundamental studies are still required to fully realize their potential. Specifically, there is still not a fundamental understanding to how AC interaction with polymers can be probed before membrane formation. Classic methods for probing interaction in other cases involve comparing solubility parameters and analyzing functional groups. However, in the case of solid-liquid and solid-solid interactions involving AC, this becomes more complex, and determining solubility parameters becomes difficult. Therefore, fundamental studies are needed to expose the mechanism behind AC interactions with polymers, solvents, and other additives. This will involve the development of novel methods and perhaps the theoretical framework from colloid interactions in various media.

Another fundamental necessity that is thus far unclear is a relationship between AC properties and MMM performance. There is contradictory evidence between AC surface area, pore size, particle size and functionality on MMM performance. This lends to the conclusion there is ample interactions between each property that is not yet realized. Understanding this would require studies with carefully controlled AC properties be pursued, which can be accomplished by investigating various biomass or polymer precursors, activating methods, and post treatments. This fundamental knowledge would provide some criteria and more insight into material selection of AC and polymer combinations.

In AC-MMM formation, still very little has been investigated relating phase inversion variables and MMM properties. Important variables include nonsolvent, additives, and temperature. Each is likely to cause a shift in the equilibrium between each phase in the casting solution. Binodal shifts in ternary phase diagrams can give insight into cross sectional structure and help guide experimentation, which has yet to be thoroughly examined. Detailed studies of dry phase inversion are also needed. It is not clear how various parameters can be manipulated to prevent unwanted sedimentation and surface ruptures. These studies are ultimately needed to determine if particle/filler interaction can be influenced by variables in the membrane formation process. Likewise, other membrane fabrication techniques should be investigated that may prove useful for

some applications. For example, electrospinning of AC into fibrous membranes presents a plausible scenario (164), in which applications with surface pore size sensitivity may benefit.

In applications where adsorption is a major factor in separation performance, methods to sufficiently regenerate spent AC are still needed. This is a major issue because all active sites on the AC in MMMs may not be accessible by all fluids, which restricts the regenerating ability of some chemicals. Thus, a variety of regenerating methods needs to be investigated to give insight into how effective regenerating AC-MMMs are for various ions and molecules. This will allow realization of the extend of applications in which these membranes can be employed.

Furthermore, the gas separation potential of AC-MMMs should be further pursued. This will also involve fine control of particle size distribution, pore size distribution, and surface area in AC and CMS. In doing so, AC-MMMs can be tailored to specific gas separation applications by enabling different flow regimes in the AC such as Knudsen diffusion, surface diffusion, and molecular sieving. Each may have advantages for different gas mixtures. Various other applications of AC-MMMs should also be investigated. One example is direct contact membrane distillation, which is influenced by membrane porosity, free volume, and thermal properties. Other applications involve proton exchange. While there have been some efforts to use AC-MMMs in proton exchange, their full potential has not been realized. Lastly, predictive models that take into consideration size distribution, pore size distribution, and shape distribution should be pursued. Currently no models consider variations in filler particles, but will be highly beneficial to AC-MMM due to the inevitable variability between particles. In all, these studies would benefit AC-MMMs greatly, but also provide insight into the entire class of MMMs.

9. Acknowledgements

The authors declare no conflicts of interest. This research was supported by North Dakota Department of Commerce (Fund 16-08-J1-144), NASA EPSCoR (NNX15AK49A), and ND EPSCoR (FAR0023660). The authors would like to acknowledge valuable communication with Essam Aljundi, KFUPM for his insight into AC-polymer interactions, and membrane surface chemistry as well as Elio Gonzo, INIQUI, and Vinh Hoang, Laval University, for their insight into predictive models, specifically the GPG model and its derivation.

10. References

1. Paul, D. R. and Kemp,D. R. (1973) The Difussion Time Lag in Polymer Membranes Containing Adsorptive Fillers. *J. Polym. Sci. Polym. Symp.,* 41:79-93.

2. Drioli, E. and Giorno, L. (2016) *Encyclopedia of Membranes.* Springer: Verlag Berlin Heidelberg.

3. Baghbanzadeh, M., Rana, D., Lan, C.Q., and Matsuura, T. (2016) Effects of Inorganic Nano-Additives on Properties and Performance of Polymeric Membranes in Water Treatment. *Sep. Purif. Rev.,* 45: 141-167. doi:10.1080/15422119.2015.1068806

4. Villalobos-Rodríguez, R., Montero-Cabrera, M.E., Esparza-Ponce, H.E., Herrera-Peraza, E.F., and Ballinas-Casarrubias, M.L. (2012) Uranium Removal from Water using Cellulose Triacetate Membranes Added with Activated Carbon. *Appl. Radiat. Isot.,* 70: 872-881. doi:10.1016/j.apradiso.2012.01.017

5. Nejad, M.N., Asghari, M., and Afsari, M. (2016) Investigation of Carbon Nanotubes in Mixed Matrix Membranes for Gas Separation: A Review. *ChemBioEng Rev.,* 3: 276-298. doi:10.1002/cben.201600012

6. Dechnik, J., Sumby, C.J., and Janiak, C. (2017) Enhancing Mixed-Matrix Membrane Performance with Metal–Organic Framework Additives. *Cryst. Growth Des.,* 17: 4467-4488. doi:10.1021/acs.cgd.7b00595

7. Vu, D.Q., Koros, W.J. and Miller, S.J. (2003) Mixed Matrix Membranes using Carbon Molecular Sieves: I. Preparation and Experimental Results. *J. Membr. Sci.,* 211: 311-334. doi:10.1016/S0376-7388(02)00429-5

8. Vu, D.Q., Koros, W.J. and Miller, S.J. (2003) Mixed Matrix Membranes using Carbon Molecular Sieves: II. Modeling Permeation Behavior. *J. Membr. Sci.,* 211: 335-348. doi:10.1016/S0376-7388(02)00425-8

9. Muntha, S.T., Kausar, A., and Siddiq, M. (2016) A Review on Zeolite-Reinforced Polymeric Membranes: Salient Features and Applications. *Polym. Plast. Technol. Eng.,* 55: 1971-1987. doi:10.1080/03602559.2016.1185631

10. Weigelt, F., Georgopanos, P., Shishatskiy, S., Filiz, V., Brinkmann, T., and Abetz, V. (2018) Development and Characterization of Defect-Free Matrimid Mixed-Matrix Membranes Containing Activated Carbon Particles for Gas Separation. *Polymers,* 10:1-21. doi:10.3390/polym10010051

11. Tessema, T.D.M., Venna, S.R., Dahe, G., Hopkinson, D.P., El-Kaderi, H.M., and Sekizkardes, A.K. (2018) Incorporation of Benzimidazole Linked Polymers into Matrimid to Yield Mixed Matrix Membranes with Enhanced CO 2 /N 2 Selectivity. *J. Membr. Sci.,* 554: 90-96. doi:10.1016/j.memsci.2018.02.054

12. Rezaee, R., Nasseri, S., Mahvi, A.H., Nabizadeh, R., Mousavi, S.A., Rashidi, A., Jafari, A., and Nazmara, S. (2015) Fabrication and Characterization of a Polysulfone-Graphene Oxide Nanocomposite Membrane for Arsenate Rejection from Water. *J. Environ. Health Sci. Eng.,* 13:61. doi:10.1186/s40201-015-0217-8

13. Mukherjee, R., and De, S. (2016) Novel Carbon-Nanoparticle Polysulfone Hollow Fiber Mixed Matrix Ultrafiltration Membrane: Adsorptive Removal of Benzene, Phenol and Toluene from Aqueous Solution. *Sep. Purif. Technol.,* 157: 229-240. doi:10.1016/j.seppur.2015.11.015

14. Anadão, P., Sato, L.F., Wiebeck, H., and Valenzuela-Díaz, F.R. (2010) Polysulfone Activated Carbon Composite Membranes. *Mater. Sci. Forum,* 660-661: 1081-1086. doi:10.4028/www.scientific.net/MSF.660-661.1081

15. Anson, M., Marchese, J., Garis, E., Ochoa, N., and Pagliero, C. (2004) ABS Copolymer-Activated Carbon Mixed Matrix Membranes for CO2/CH4 Separation. *J. Membr. Sci.,* 243: 19-28. doi:10.1016/j.memsci.2004.05.008

16. Fu, X., Maruyama, T., Sotani, T., and Matsuyama, H. (2008) Effect of Surface Morphology on Membrane Fouling by Humic Acid with the use of Cellulose Acetate Butyrate Hollow Fiber Membranes. *J. Membr. Sci.,* 320: 483-491. doi:10.1016/j.memsci.2008.04.027

17. Aroon, M. A., Ismail, A.F., Matsuura, T. and Montazer-Rahmati, M.M. (2010) Performance Studies of Mixed Matrix Membranes for Gas Separation: A Review. *Sep. Purif. Technol.,* 75: 229-242. doi:10.1016/j.seppur.2010.08.023

18. Goh, P.S., Ismail, A.F., Sanip, S.M., Ng, B.C., and Aziz, M. (2011) Recent Advances of Inorganic Fillers in Mixed Matrix Membrane for Gas Separation. *Sep.Purif. Technol.,* 81: 243-264. doi:10.1016/j.seppur.2011.07.042

19. Chung, T., Jiang, L.Y., Li, Y., and Kulprathipanja, S. (2007) Mixed Matrix Membranes (MMMs) Comprising Organic Polymers with Dispersed Inorganic Fillers for Gas Separation. *Prog. Polym. Sci.,* 32: 483-507. doi:10.1016/j.progpolymsci.2007.01.008

20. Rezakazemi, M., Amooghin, A.E., Montazer-Rahmati, M.M., Ismail, A.F., and Matsuura, T. (2014) State-of-the-Art Membrane Based CO.Sub.2 Separation using Mixed Matrix Membranes : An Overview on Current Status and Future Directions. *Prog. Polym. Sci.,* 39: 817. doi:10.1016/j.progpolymsci.2014.01.003

21. Vinoba, M., Bhagiyalakshmi,M., Alqaheem,Y., Alomair,A. A., Pérez,A. and Rana,M. S. (2017) Recent Progress of Fillers in Mixed Matrix Membranes for CO2 Separation: A Review. *Sep. Purif. Technol.,* 188: 431-450. doi:10.1016/j.seppur.2017.07.051

22. Goh. P.S., Ng B.C., Lau, W.J. and Ismail, A.F. (2014) Inorganic Nanomaterials in Polymeric Ultrafiltration Membranes for Water Treatment. *Sep. Purif. Rev.,* 44: 216-249. doi:10.1080/15422119.2014.926274

23. Qadir D., Mukhtar, H., and Keong L.K. (2016) Mixed Matrix Membranes for Water Purification Applications. *Sep. Purif. Rev.,* 46: 62-80. doi:10.1080/15422119.2016.1196460

24. Bastani, D., Esmaeili, N., and Asadollahi, M. (2013) Polymeric Mixed Matrix Membranes Containing Zeolites as a Filler for Gas Separation Applications: A Review. *J. Ind. Eng. Chem.,* 19: 375-393. doi:10.1016/j.jiec.2012.09.019

25. Lakhotia, S. R., Mukhopadhyay, M., and Kumari, P. (2017) Surface-Modified Nanocomposite Membranes. *Sep. Purif. Rev.,* 47: 288-305. doi:10.1080/15422119.2017.1386681

26. Liu, M., Gurr, P.A., Fu, Q., Webley, P.A., and Qiao, G.G. (2018) Two-Dimensional Nanosheet-Based Gas Separation Membranes. *J. Mater. Chem. A,* 6: 23169-23196. doi:10.1039/c8ta09070j

27. Cheng, Y., Ying, Y., Japip, S., Jiang, S., Chung, T., Zhang, S., and Zhao, D. (2018) Advanced Porous Materials in Mixed Matrix Membranes. *Adv. Mater.,* 30: 1802401. doi:10.1002/adma.201802401

28. Ismail, A. F., Khulbe, K.C., and Matsuura, T. (2015) *Gas Separation Membranes.* Springer International Publishing: Cham.

29. Al-Sayaghi, M., Lewis, J., Buelke, C., and Alshami, A.S. (2018) Physicochemical and Thermal Effects of Pendant Groups, Spatial Linkages and Bridging Groups on the Formation and Processing of Polyimides. *Int. J. Polym. Anal. Charact.,* 23: 566-576. doi:10.1080/1023666X.2018.1505221

30. Mallade, R., and Menendez, M. (2008) *Inorganic Membranes.* Elsevier Science: San Diego, CA, USA.

31. Hinds, B. J., Chopra, N., Rantell, T., Andrews, R., Gavalas, V., and Bachas, L.G. (2004) Aligned Multiwalled Carbon Nanotube Membranes. *Science,* 303: 62-65. doi:10.1126/science.1092048

32. Buelke, C., Alshami, A., Casler, J., Lewis, J., Al-Sayaghi, M., and Hickner, M.A. (2018) Graphene Oxide Membranes for Enhancing Water Purification in Terrestrial and Space-Born Applications: State of the Art. *Desalination,* doi:10.1016/j.desal.2018.09.008

33. Marino, T., Russo, F., Rezzouk, L., Bouzid, A., and Figoli, A. (2017) PES-Kaolin Mixed Matrix Membranes for Arsenic Removal from Water. *Membranes,* 7: 57. doi:10.3390/membranes7040057

34. Penkova, A.V., Dmitrenko, M.E., Savon, N.A., Missyul, A.B., Mazur, A.S., Kuzminova, A.I., Zolotarev, A.A., Mikhailovskii, V., Lahderanta, E., Markelov, D.A., Semenov, K.N., and Ermakov, S.S. (2018) Novel Mixed-

Matrix Membranes Based on Polyvinyl Alcohol Modified by Carboxyfullerene for Pervaporation Dehydration. *Sep. Purif. Technol.,* 204: 1-12. doi:10.1016/j.seppur.2018.04.052

35. Ishaq, S., Tamime, R., Bilad, M.R., and Khan, A.L. (2019) Mixed Matrix Membranes Comprising of Polysulfone and Microporous Bio-MOF-1: Preparation and Gas Separation Properties. *Sep. Purif. Technol.,* 210: 442-451. doi:10.1016/j.seppur.2018.08.031

36. Anisuzzaman, S.M., Joseph, C.G., Taufiq-Yap, Y.H., Krishnaiah, D., and Tay, V.V. (2015) Modification of Commercial Activated Carbon for the Removal of 2,4-Dichlorophenol from Simulated Wastewater. *JKSUS.,* 27: 318-330. doi:10.1016/j.jksus.2015.01.002

37. Ahmad, M., Rajapaksha, A.U., Lim, J.E., Zhang, M., Bolan, N., Mohan, D., Vithanage, M., Lee, S.S., and Ok, Y.S. (2014) Biochar as a Sorbent for Contaminant Management in Soil and Water: A Review. *Chemosphere,* 99: 19-33. doi:10.1016/j.chemosphere.2013.10.071

38. Sharma, A., Pareek, V., and Zhang, D. (2015) Biomass pyrolysis—A Review of Modelling, Process Parameters and Catalytic Studies. *Renew. Sust. Energ. Rev.,* 50: 1081-1096. doi:10.1016/j.rser.2015.04.193

39. Efika, C.E., Onwudili, J.A., and Williams, P.T. (2018) Influence of Heating Rates on the Products of High-Temperature Pyrolysis of Waste Wood Pellets and Biomass Model Compounds. *Waste Manage.,* 76: 497-506. doi:10.1016/j.wasman.2018.03.021

40. Guedes, R.E., Luna, A.S., and Torres, A.R. (2018) Operating Parameters for Bio-Oil Production in Biomass Pyrolysis: A Review. *J. Anal. Appl. Pyrolysis,* 129: 134-149. doi:10.1016/j.jaap.2017.11.019

41. Mohan, D., Pittman, C.U., and Steele, P.H. (2006) Pyrolysis of Wood/Biomass for Bio-Oil: A Critical Review. *Energy Fuels,* 20: 848-889. doi:10.1021/ef0502397

42. Han, J., and Kim, H. (2008) The Reduction and Control Technology of Tar during Biomass Gasification/Pyrolysis: An Overview. *Renew. Sust. Energ. Rev.,* 12: 397-416. doi:10.1016/j.rser.2006.07.015

43. Kandel, K., Koc-Karabocek, R., Xu, T., Wang, F.C.Y., and Ferrughelli, D.T. (2018) Upgrading Hydrocarbon Pyrolysis Tar. US20180057759A1

44. Tesser, A., Alemaryeen, A., Lewis, J., Alshami, A., Haghshenas, M., Noghanian, S. PLA-biotar composite substrate for an RF antenna. *In preparation for Sci. Rep.*

45. Xu, T., Lou, L., Luo, L., Cao, R., Duan, D., and Chen, Y. (2012) Effect of Bamboo Biochar on Pentachlorophenol Leachability and Bioavailability in Agricultural Soil. *Sci. Total Environ.,* 414: 727-731. doi:10.1016/j.scitotenv.2011.11.005

46. Ahmad, M., Lee, S.S., Dou, X., Mohan, D., Sung, J., Yang, J.E., and Ok, Y.S. (2012) Effects of Pyrolysis Temperature on Soybean Stover- and Peanut Shell-Derived Biochar Properties and TCE Adsorption in Water. *Bioresour. Technol.,* 118: 536-544. doi:10.1016/j.biortech.2012.05.042

47. Ahmad, M., Lee, S., Lee, S.S., Rajapaksha, A.U., Vithanage, M., Zhang, M., Cho, J.S., and Ok, Y.S. (2013) Trichloroethylene Adsorption by Pine Needle Biochars Produced at various Pyrolysis Temperatures. *Bioresour. Technol.,* 143: 615-622. doi:10.1016/j.biortech.2013.06.033

48. Weber, K., and Quicker, P. (2018) Properties of Biochar. *Fuel,* 217: 240-261. doi:10.1016/j.fuel.2017.12.054

49. Liu, W.J., Jiang, H., and Yu, H.Q. (2015) Development of Biochar-Based Functional Materials: Toward a Sustainable Platform Carbon Material. *Chem. Rev.,* 115 :12251-12285. doi:10.1021/acs.chemrev.5b00195

50. Idrees, M., Batool, S., Kalsoom, T., Kalsoom, A., Yasmeen, S., Raina, S., Zhuang, Q., and Kong, J. (2018) Animal Manure-Derived Biochars Produced Via Fast Pyrolysis for the Removal of Divalent Copper from Aqueous Media. *J. Environ. Manage.,* 213: 109-118. doi:10.1016/j.jenvman.2018.02.003

51. Abdelhafez, A.A., and Li, J. (2016) Removal of Pb(II) from Aqueous Solution by using Biochars Derived from Sugar Cane Bagasse and Orange Peel. *J. Taiwan Inst. Chem. Eng.,* 61: 367-375. doi:10.1016/j.jtice.2016.01.005

52. Saleh, M.E., El-Refaey, A.A., and Mahmoud, A.H. (2016) Effectiveness of Sunflower Seed Husk Biochar for Removing Copper Ions from Wastewater: A Comparative Study. *Soil Water Res.,* 11: 53-63. doi:10.17221/274/2014-SWR

53. Usman, A.R.A., Abduljabbar, A., Vithanage, M., Ok, Y.S., Ahmad, M., Ahmad, M., Elfaki, J., Abdulazeem, S.S., and Al-Wabel, M.I. (2015) Biochar Production from Date Palm Waste: Charring Temperature Induced Changes in Composition and Surface Chemistry. *J. Anal. Appl. Pyrolysis,* 115: 392-400. doi:10.1016/j.jaap.2015.08.016

54. Zielinska, A., and Oleszczuk, P. (2015) Evaluation of Sewage Sludge and Slow Pyrolyzed Sewage Sludge-Derivedbiochar for Adsorption of Phenanthrene and Pyrene. *Bioresour. Technol.,* 192: 618-626. doi:10.1016/j.biortech.2015.06.032

55. Xu, X., Cao, X., and Zhao, L. (2013) Comparison of Rice Husk- and Dairy Manure-Derived Biocharsfor Simultaneously Removing Heavy Metals from Aqueous Solutions: Role of Mineral Components in Biochars. *Chemosphere,* 92: 955-961. doi:10.1016/j.chemosphere.2013.03.009

56. Shen, Y., Wang, S., Tzou, Y., Yan, Y., and Kuan, W. (2012) Removal of Hexavalent Cr by Coconut Coir and Derived Chars – the Effect of Surface Functionality. *Bioresour. Technol.,* 104: 165-172. doi:10.1016/j.biortech.2011.10.096

57. Wang. B., Lehmann, J., Hanley, K., Hestrin, R., and Enders, A. (2015) Adsorption and Desorption of Ammonium by Maple Wood Biocharas a Function of Oxidation and pH. *Chemosphere,* 138: 120-126. doi:10.1016/j.chemosphere.2015.05.062

58. Sun, L., Chen, D., Wan, S., and Yu, Z. (2015) Performance, Kinetics, and Equilibrium of Methylene Blue Adsorption on Biochar Derived from Eucalyptus Saw Dust Modified with Citric, Tartaric, and Acetic Acids. *Bioresour. Technol.,* 198: 300-308. doi:10.1016/j.biortech.2015.09.026

59. Meng, J., Tao, M., Wang, L., Liu, X., and Xu, J. (2018) Changes in Heavy Metal Bioavailability and Speciation from a Pb-Zn Mining Soil Amended with Biochars from Co-Pyrolysis of Rice Straw and Swine Manure. *Sci. Total Environ.,* 633: 300-307. doi:10.1016/j.scitotenv.2018.03.199

60. Luo, M., Lin, H., Li, B., Dong, Y., He, Y., and Wang, L. (2018) A Novel Modification of Lignin on Corncob-Based Biochar to Enhance Removal of Cadmium from Water. *Bioresour. Technol.,* 259: 312-318. doi:10.1016/j.biortech.2018.03.075

61. Yang, X., Kwon, E.E., Dou, X., Zhang, M., Kim, K., Tsang, D.C.W., and Ok, Y.S. (2018) Fabrication of Spherical Biochar by a Two-Step Thermal Process from Waste Potato Peel. *Sci. Total Environ.,* 626: 478-485. doi:10.1016/j.scitotenv.2018.01.052

62. Elleuch, A., Boussetta, A., Yu, J., Halouani, K., and Li, Y. (2013) Experimental Investigation of Direct Carbon Fuel Cell Fueled by Almond Shell Biochar: Part I. Physico-Chemical Characterization of the Biochar Fuel and Cell Performance Examination. *Int. J. Hydrogen Energy,* 38: 16590-16604. doi:10.1016/j.ijhydene.2013.08.090

63. Zhang, T., Walawender, W. P., Fan, L. T., Fan, M., Daugaard, D., and Brown, R.C. (2004) Preparation of Activated Carbon from Forest and Agricultural Residues through CO2 Activation. *Chem. Eng. J.,* 105: 53-59. doi:10.1016/j.cej.2004.06.011

64. Shim, T., Yoo, J., Ryu, C., Park, Y., and Jung, J. (2015) Effect of Steam Activation of Biochar Produced from a Giant Miscanthus on Copper Sorption and Toxicity. *Bioresour. Technol.,* 197: 85-90. doi:10.1016/j.biortech.2015.08.055

65. Xiao, F., Bedane, A.H., Zhao, J.X., Mann, M.D., and Pignatello, J.J. (2018) Thermal Air Oxidation Changes Surface and Adsorptive Properties of Black Carbon (Char/Biochar). *Sci. Total Environ.,* 618: 276-283. doi:10.1016/j.scitotenv.2017.11.008

66. Ioannidou, O., and Zabaniotou, A. (2007) Agricultural Residues as Precursors for Activated Carbon production-A Review. *Renew. Sust. Energ Rev.,* 11: 1966-2005. doi:10.1016/j.rser.2006.03.013

67. Dehkhoda, A.M., Gyenge, E., and Ellis, N. (2016) A Novel Method to Tailor the Porous Structure of KOH-Activated Biochar and its Application in Capacitive Deionization and Energy Storage. *Biomass Bioenergy,* 87: 107-121. doi:10.1016/j.biombioe.2016.02.023

68. Islam, M.A., Tan, I.A.W., Benhouria, A., Asif, M., and Hameed, B.H. (2015) Mesoporous and Adsorptive Properties of Palm Date Seed Activated Carbon Prepared Via Sequential Hydrothermal Carbonization and Sodium Hydroxide Activation. *Chem.l Eng. J.,* 270: 187-195. doi:10.1016/j.cej.2015.01.058

69. Aljeboree, A.M., Alshirifi, A.N. and Alkaim, A.F. (2017) Kinetics and Equilibrium Study for the Adsorption of Textile Dyes on Coconut Shell Activated Carbon. *Arab. J. Chem.,* 10: S3393. doi:10.1016/j.arabjc.2014.01.020

70. Demiral, H., and Gungor, C. (2016) Adsorption of Copper(II) from Aqueous Solutions on Activated Carbon Prepared from Grape Bagasse. *J. Clean. Prod.,* 124: 103-113. doi:10.1016/j.jclepro.2016.02.084

71. Ozdemir, I., Şahin, M., Orhan, R., and Erdem, M. (2014) Preparation and Characterization of Activated Carbon from Grape Stalk by Zinc Chloride Activation. *Fuel Process. Technol.,* 125: 200-206. doi:10.1016/j.fuproc.2014.04.002

72. Muniandy, L., Adam, F., Mohamed, A.R., and Ng, E. (2014) The Synthesis and Characterization of High Purity Mixed Microporous/Mesoporous Activated Carbon from Rice Husk using Chemical Activation with NaOH and KOH. *Microporous Mesoporous Mater.,* 197: 316-323. doi:10.1016/j.micromeso.2014.06.020

73. Liou, T.H. (2010) Development of Mesoporous Structure and High Adsorption Capacity of Biomass-Based Activated Carbon by Phosphoric Acid and Zinc Chloride Activation. *Chem. Eng. J.,* 158: 129-142. doi:10.1016/j.cej.2009.12.016

74. Nayak, A., Bhushan, B., Gupta, V., and Sharma, P. (2017) Chemically Activated Carbon from Lignocellulosic Wastes for Heavy Metal Wastewater Remediation: Effect of Activation Conditions. *J. Colloid Interface Sci.,* 493: 228-240. doi:10.1016/j.jcis.2017.01.031

75. Yorgun, S., and Yıldız, D. (2015) Preparation and Characterization of Activated Carbons from Paulownia Wood by Chemical Activation with H3PO4. *J. Taiwan Inst. Chem. Eng.,* 53: 122-131. doi:10.1016/j.jtice.2015.02.032

76. Iriarte-Velasco, U., Sierra, I., Cepeda, E.A., Bravo, R., and Ayastuy, J.L. (2015) Methylene Blue Adsorption by Chemicallyactivated Waste Pork Bones. *Color. Technol.,* 131: 322-332. doi:10.1111/cote.12160

77. Kiyono, M., Williams, P.J., and Koros, W.J. (2010) Effect of Pyrolysis Atmosphere on Separation Performance of Carbon Molecular Sieve Membranes. *J. Membr. Sci.,* 359: 2-10. doi:10.1016/j.memsci.2009.10.019

78. Hassan, M., Abou-Zeid, R., Hassan, E., Berglund, L., Aitomäki, Y., and Oksman, K. (2017) Membranes Based on Cellulose Nanofibers and Activated Carbon for Removal of Escherichia Coli Bacteria from Water. *Polymers,* 9: 335. doi:10.3390/polym9080335

79. Mushardt, H., Müller, M., Shishatskiy, S., Wind, J., and Brinkmann, T. (2016) Detailed Investigation of Separation Performance of a MMM for Removal of Higher Hydrocarbons Under Varying Operating Conditions. *Membranes,* 6:16. doi:10.3390/membranes6010016

80. Tanco, M.A.L., and Tanaka, D.A.P. (2016) Recent Advances on Carbon Molecular Sieve Membranes (CMSMs) and Reactors. *Processes,* 4: 29. doi:10.3390/pr4030029

81. Nasir, R., Mukhtar, H., Man, Z., Dutta, B.K., Shaharun, M.S., and Abu Bakar, M.Z. (2015) Mixed Matrix Membrane Performance Enhancement using Alkanolamine Solution. *J. Membr. Sci.,* 483: 84-93. doi:10.1016/j.memsci.2015.02.041

82. Dong, G., Li, H., and Chen, V. (2013) Challenges and Opportunities for Mixed-Matrix Membranes for Gas Separation. *J. Mater. Chem. A,* 1: 4610. doi:10.1039/c3ta00927k

83. Jia, M., Pleinemann, K., and Behling, R. (1992) Preparation and Characterization of Thin-Film zeolite–PDMS Composite Membranes. *J. Membr. Sci.,* 73: 119-128. doi:10.1016/0376-7388(92)80122-Z

84. Torras, C., Ferrando, F., Paltakari, J., and Garcia-Valls, R. (2006) Performance, Morphology and Tensile Characterization of Activated Carbon Composite Membranes for the Synthesis of Enzyme Membrane Reactors. *J. Membr. Sci.,* 282: 149-161. doi:10.1016/j.memsci.2006.05.018

85. Galizia, M., Chi, W.S., Smith, Z.P., Merkel, T.C., Baker, R.W., and Freeman, B.D. (2017) 50th Anniversary Perspective: Polymers and Mixed Matrix Membranes for Gas and Vapor Separation: A Review and Prospective Opportunities. *Macromolecules,* 50: 7809-7843. doi:10.1021/acs.macromol.7b01718

86. Nasir, R., Mukhtar, H., Man, Z. and Mohshim, D.F. (2013) Material Advancements in Fabrication of Mixed-Matrix Membranes. *Chem. Eng. Technol.,* 36: 717-727. doi:10.1002/ceat.201200734

87. Michele, L.D., Zaccone, A., and Eiser, E. (2012) Analytical Theory of Polymer-Network-Mediated Interaction between Colloidal Particles. *Proc. Natl. Acad. Sci. USA.* 109: 10187-10192. doi:10.1073/pnas.1202171109

88. Bar-Chaput, S. and Carrot, C. (2006) Interactions of Active Carbon with Low- and High-molecular Weight Polyethylene Glycol and Polyethylene Oxide. *J. Appl. Polym. Sci.,* 100: 3490-3497. doi:10.1002/app.22149

89. Mushardt, H., Kramer, V., Hülagü, D., Brinkmann, T., and Kraume, M. (2014) Development of Solubility Selective Mixed Matrix Membranes for Gas Separation. *Chem. Ing. Tech.,* 86: 83-91. doi:10.1002/cite.201300074

90. García, M.G., Marchese, J., and Ochoa, N.A. (2010) Effect of the Particle Size and Particle Agglomeration on Composite Membrane Performance. *J. Appl. Polym. Sci.,* 118: 2417-2424. doi:10.1002/app.32274

91. Mukherjee, R., and De, S. (2016) Preparation, Characterization and Application of Powdered Activated Carbon-cellulose Acetate Phthalate Mixed Matrix Membrane for Treatment of Steel Plant Effluent. *Polym. Adv. Technol.,* 27: 444-459. doi:10.1002/pat.3690

92. Kusworo, T.D., Ismail, A.F., Mustafa, A., and Budiyono. (2010) Application of Activated Carbon Mixed Matrix Membrane for Oxygen Purification. *Int. J. Sci. Eng.,* 1: 21-24.

93. Kumar, S.K., Li, C., Schadler, L.S., Bansal, A., Cho, K., Yang, H., and Benicewicz, B.C. (2005) Quantitative Equivalence between Polymer Nanocomposites and Thin Polymer Films. *Nat. Mat.,* 4: 693-698. doi:10.1038/nmat1447

94. Lin, R., Villacorta Hernandez, B., Ge, L., and Zhu, Z. (2018) Metal Organic Framework Based Mixed Matrix Membranes: An Overview on Filler/Polymer Interfaces. *J. Mater. Chem. A,* 6: 293-312. doi:10.1039/c7ta07294e

95. Lan, Y., and Wang, W. (2017) Application of Tree Biochar in PDMS Pervaporation Membranes. *Adv. Polym. Technol.,* doi:10.1002/adv.21856

96. Mohshim, D.F., Mukhtar, H., and Man, Z. (2014) The Effect of Incorporating Ionic Liquid into Polyethersulfone-SAPO34 Based Mixed Matrix Membrane on CO2 Gas Separation Performance. *Sep. Purif. Technol.,* 135: 252-258. doi:10.1016/j.seppur.2014.08.019

97. Mohshim, D.F., Mukhtar, H.B., Man, Z., and Nasir, R. (2013) Latest Development on Membrane Fabrication for Natural Gas Purification: A Review. *J. Eng.,* 2013: 1-7. doi:10.1155/2013/101746

98. Ebadi Amooghin, A., Mashhadikhan, S., Sanaeepur, H., Moghadassi, A., Matsuura, T., and Ramakrishna, S. (2019) Substantial Breakthroughs on Function-Led Design of Advanced Materials used in Mixed Matrix Membranes (MMMs): A New Horizon for Efficient CO2 Separation. *Prog. Mater. Sci.,* 102: 222-295. doi:10.1016/j.pmatsci.2018.11.002

99. Saranya, R., Kumar, M., Tamilarasan, R., Ismail, A.F., and Arthanareeswaran, G. (2016) Functionalised Activated Carbon Modified Polyphenylsulfone Composite Membranes for Adsorption Enhanced Phenol Filtration. *J. Chem. Technol. Biotechnol.,* 91: 748-761. doi:10.1002/jctb.4641

100. Spahis, N., Dellali, M., and Mahmoudi, H. (2012) Synthesis and Characterization of Polymeric/Activated Carbon Membranes. *Procedia Eng.,* 33: 47-51. doi:10.1016/j.proeng.2012.01.1175

101. Ballinas-Casarrubias, L., Terrazas-Bandala, L.P., Ibarra-Gomez, R., Mendoza-Duarte, M.E., Manjarrez-Nevarez, L., and Gonzalez-Sanchez, G. (2006) Structural and Performance Variation of Activated Carbon-Polymer films. *Polym. Adv. Technol.,* 17: 991-999. doi:10.1002/pat.842

102. Garcia, M., Marchese, J., and Ochoa, N. (2012) High Activated Carbon Loading Mixed Matrix Membranes for Gas Separations. *J Mater Sci,* 47: 3064-3075. doi:10.1007/s10853-011-6138-8

103. Shen, G., Zhao, J., Guan, K., Shen, J., and Jin, W. (2017) Highly Efficient Recovery of Propane by Mixed-matrix Membrane Via Embedding Functionalized Graphene Oxide Nanosheets into Polydimethylsiloxane. *AIChE J.,* 63: 3501-3510. doi:10.1002/aic.15720

104. Li, Q., Cheng, L., Shen, J., Shi, J., Chen, G., Zhao, J., Duan, J., Liu, G., and Jin, W. (2017) Improved Ethanol Recovery through Mixed-Matrix Membrane with Hydrophobic MAF-6 as Filler. *Sep.Purif. Technol.,* 178: 105-112. doi:10.1016/j.seppur.2017.01.024

105. Bakeri, G., Ismail, A.F., Shariaty-Niassar, M., and Matsuura, T. (2010) Effect of Polymer Concentration on the Structure and Performance of Polyetherimide Hollow Fiber Membranes. *J. Membr. Sci.,* 363: 103-111. doi:10.1016/j.memsci.2010.07.018

106. Ariono, D., Aryanti, P.T.P., Subagjo, S., and Wenten, I.G. (2017) The Effect of Polymer Concentration on Flux Stability of Polysulfone Membrane. *AIP Conf. Proc.,* 1788: 030048. doi:10.1063/1.4968301

107. Adewole, J.K., Ahmad, A.L., Ismail, S., Leo, C.P., and Sultan, A.S. (2015) Comparative Studies on the Effects of Casting Solvent on Physico-Chemical and Gas Transport Properties of Dense Polysulfone Membrane used for CO2/CH4separation. *J. Appl. Polym. Sci.,* 132: 42205. doi:10.1002/app.42205

108. Guillen, G.R., Pan, Y., Li, M., and Hoek, E.M.V. (2011) Preparation and Characterization of Membranes Formed by Nonsolvent Induced Phase Separation: A Review. *Ind. Eng. Chem. Res.,* 50: 3798-3817. doi:10.1021/ie101928r

109. Azimi, H., Tezel, F.H., and Thibault, J. (2017) Effect of Embedded Activated Carbon Nanoparticles on the Performance of Polydimethylsiloxane (PDMS) Membrane for Pervaporation Separation of Butanol. *J. Chem. Technol. Biotechnol.,* 92: 2901-2911. doi:10.1002/jctb.5306

110. Wan, C.F., Yang, T., Lipscomb, G.G., Stookey, D.J., and Chung, T. (2017) Design and Fabrication of Hollow Fiber Membrane Modules. *J. Membr. Sci.,* 538: 96-107. doi:10.1016/j.memsci.2017.05.047

111. Tijink, M.S.L., Wester, M., Sun, J., Saris, A., Bolhuis-Versteeg, L.A.M., Saiful, S., Joles, J.A., Borneman, Z., Wessling, M., and Stamatialis, D.F. (2012) A Novel Approach for Blood Purification: Mixed-Matrix Membranes Combining Diffusion and Adsorption in One Step. *Acta Biomater.,* 8: 2279-2287. doi:10.1016/j.actbio.2012.03.008

112. Tijink, M.S.L., Wester, M., Glorieux, G., Gerritsen, K.G.F., Sun, J., Swart, P.C., Borneman, Z., Wessling, M., Vanholder, R., Joles, J.A., and Stamatialis, D. (2013) Mixed Matrix Hollow Fiber Membranes for Removal of Protein-Bound Toxins from Human Plasma. *Biomaterials,* 34: 7819-7828. doi:10.1016/j.biomaterials.2013.07.008

113. Feng, C.Y., Khulbe, K.C., Matsuura, T., and Ismail, A.F. (2013) Recent Progresses in Polymeric Hollow Fiber Membrane Preparation, Characterization and Applications. *Sep. Purif. Technol.,* 111: 43-71. doi:10.1016/j.seppur.2013.03.017

114. Ren, J., Zhou, J., and Deng, M. (2010) Morphology Transition of Asymmetric Polyetherimide Flat Sheet Membranes with Different Thickness by Wet Phase-Inversion Process. *Sep.Purif. Technol.,* 74: 119-129. doi:10.1016/j.seppur.2010.05.014

115. Buonomenna, M.G., Figoli, A., Jansen, J.C., and Drioli, E. (2004) Preparation of Asymmetric PEEKWC Flat Membranes with Different Microstructures by Wet Phase Inversion. *J. Appl. Polym. Sci.,* 92: 576-591. doi:10.1002/app.20042

116. Sadrzadeh, M., and Bhattacharjee, S. (2013) Rational Design of Phase Inversion Membranes by Tailoring Thermodynamics and Kinetics of Casting Solution using Polymer Additives. *J. Membr. Sci.,* 441: 31-44. doi:10.1016/j.memsci.2013.04.009

117. Garcia-Ivars, J., Iborra-Clar, M., Alcaina-Miranda, M., and Van der Bruggen, B. (2015) Comparison between Hydrophilic and Hydrophobic Metal Nanoparticles on the Phase Separation Phenomena during Formation of Asymmetric Polyethersulphone Membranes. *J. Membr. Sci.,* 493: 709-722. doi:10.1016/j.memsci.2015.07.009

118. Mazinani, S., Darvishmanesh, S., Ehsanzadeh, A. and Van der Bruggen, B. (2017) Phase Separation Analysis of Extem/Solvent/Non-Solvent Systems and Relation with Membrane Morphology. *J. Membr. Sci.,* 526: 301-314. doi:10.1016/j.memsci.2016.12.031

119. Dahe, G.J., Singh, R.P., Dudeck, K.W., Yang, D., Berchtold, K.A. (2019) Influence of non-solvent chemistry on polybenzimidazole hollow fiber membrane preparation. *J. Membr. Sci.,* 577: 91-103. doi:10.1016/j.memsci.2019.02.001

120. Hwang L.L., Chen, J.C., and Wey, M.Y. (2013) The Properties and Filtration Efficiency of Activated Carbon Polymer Composite Membranes for the Removal of Humic Acid. *Desalination,* 313: 166-175. doi:10.1016/j.desal.2012.12.019

121. Aghili, F., Ghoreyshi, A.A., Rahimpour, A., and Rahimnejad, M. (2017) Coating of Mixed-Matrix Membranes with Powdered Activated Carbon for Fouling Control and Treatment of Dairy Effluent. *Process Saf. Environ. Prot.,* 107: 528-539. doi:10.1016/j.psep.2017.03.013

122. He, J., Song, Y., and Chen, J.P. (2017) Development of a Novel Biochar/PSF Mixed Matrix Membrane and Study of Key Parameters in Treatment of Copper and Lead Contaminated Water. *Chemosphere,* 186: 1033-1045. doi:10.1016/j.chemosphere.2017.07.028

123. Hosseini, S.M., Amini, S.H., Khodabakhshi, A.R., Bagheripour, E., and Van der Bruggen, B. (2018) Activated Carbon Nanoparticles Entrapped Mixed Matrix Polyethersulfone Based Nanofiltration Membrane for Sulfate and Copper Removal from Water. *J. Taiwan Inst. Chem. Eng.,* 82: 169-178. doi:10.1016/j.jtice.2017.11.017

124. Marchese, J., Anson, M., Ochoa, N.A., Prádanos, P., Palacio, L., and Hernandez, A. (2006) Morphology and Structure of ABS Membranes Filled with Two Different Activated Carbons. *Chem. Eng. Sci.,* 61: 5448-5454. doi:10.1016/j.ces.2006.04.013

125. Soroko, I., Makowski, M., Spill, F., and Livingston, A. (2011) The Effect of Membrane Formation Parameters on Performance of Polyimide Membranes for Organic Solvent Nanofiltration (OSN). Part B: Analysis of Evaporation Step and the Role of a Co-Solvent. *J. Membr. Sci.,* 381: 163-171. doi:10.1016/j.memsci.2011.07.028

126. Gorgojo, P., Karan, S., Wong, H.C., Jimenez-Solomon, M.F., Cabral, J.T., and Livingston, A.G. (2014) Membranes: Ultrathin Polymer Films with Intrinsic Microporosity: Anomalous Solvent Permeation and High Flux Membranes. *Adv. Funct. Mater.,* 24: 4728. doi:10.1002/adfm.201470198

127. Woock, T.W. (2016) Effect of Bridging Group of Dianhydride Precursor on Resulting Thermally Rearranged Polybenzoxazole for Removal of Nitrogen from Natural Gas. *ProQuest Dissertations Publishing*.

128. Farahani, M.H.D.A., Hua, D., and Chung, T.S. (2018) Cross-Linked Mixed Matrix Membranes (MMMs) Consisting of Amine-Functionalized Multi-Walled Carbon Nanotubes and P84 Polyimide For organic Solvent Nano Filtration (OSN) with Enhanced Flux. *J. Membr. Sci.,* 548: 319-331. doi:10.1016/j.memsci.2017.11.037

129. Tashvigh, A.A., Luo, L., Chung, T.S., Weber, M., and Maletzko, C. (2018) A Novel Ionically Cross-Linked Sulfonated Polyphenylsulfone (sPPSU) Membrane for Organic Solvent Nanofiltration (OSN). *J. Membrane Sci.,* 545: 221-228. doi:10.1016/j.memsci.2017.09.076

130. Pinnau, I. and Koros, W.J. (1991) Structures and Gas Separation Properties of Asymmetric Polysulfone Membranes made by Dry, Wet, and Dry/Wet Phase Inversion. *J. Appl. Polym. Sci.,* 43: 1491-1502. doi:10.1002/app.1991.070430811

131. Snoeyink, V.L., and Weber, W.J. (1967) The Surface Chemistry of Active Carbon; a Discussion of Structure and Surface Functional Groups. *Environ. Sci. Technol.,* 1: 228-234. doi:10.1021/es60003a003

132. Ganesh, B.M., Isloor, A.M., and Ismail, A.F. (2013) Enhanced Hydrophilicity and Salt Rejection Study of Graphene Oxide-Polysulfone Mixed Matrix Membrane. *Desalination,* 313: 199-207. doi://doi.org/10.1016/j.desal.2012.11.037

133. Rahimpour, A., Madaeni, S.S., Jahanshahi, M., Mansourpanah, Y., and Mortazavian, N. (2009) Development of High Performance Nano-Porous Polyethersulfone Ultrafiltration Membranes with Hydrophilic Surface and Superior Antifouling Properties. *Appl. Surf. Sci.,* 255: 9166-9173. doi:10.1016/j.apsusc.2009.06.123

134. Rahimpour, A., Madaeni, S.S., and Mansourpanah, Y. (2007) The Effect of Anionic, Non-Ionic and Cationic Surfactants on Morphology and Performance of Polyethersulfone Ultrafiltration Membranes for Milk Concentration. *J. Membr. Sci.,* 296: 110-121. doi:10.1016/j.memsci.2007.03.029

135. Mohamad Said, K.A., George, G.G., Mohamed Alipah, N.A., Ismail, N.Z., Jamain, R.L., Mili, N., Salleh, S.F., Mohamed Amin, M.A., Muslimen, R., Yakub, I., and Mohamed Sutan, N. (2017) Effect of Activated Carbon in Polysufone-Polyethyleneimine-Silver Composite Membrane Towards Adsorption of Chromium (Cr), Lead (Pb), Silver (Ag) and Cadmium (Cd) in Synthetic Wastewater. *J. Mater. Environ. Sci.,* 8: 3740-3746.

136. Hofman, M., and Pietrzak, R. (2013) Copper Ions Removal from Liquid Phase by Polyethersulfone (PES) Membranes Functionalized by Introduction of Carbonaceous Materials. *Chem. Eng. J.,* 215-216: 216-221. doi:10.1016/j.cej.2012.10.079

137. Belgacem, A., Rebiai, R., Hadoun, H., Khemaissia, S., and Belmedani, M. (2014) The Removal of Uranium (VI) from Aqueous Solutions onto Activated Carbon Developed from Grinded used Tire. *Environ. Sci. Pollut. Res.,* 21: 684-694. doi:10.1007/s11356-013-1940-2

138. Villalobos-Rodríguez, R., Ruíz Cuilty, K., Montero-Cabrera, M.E., Esparza-Ponce, H.E., Nevarez-Moorillon, G.V., Fierro, V., Celzard, A., and Ballinas-Casarrubias, M.L. (2015) Iron Influence on Uranium Removal from Water using Cellulose Acetate Membranes Doped with Activated Carbon. *Desal. Water Treat.,* 56: 3476-3485. doi:10.1080/19443994.2014.980333

139. Sridhar, S., Smitha, B., Suryamurali, R., and Aminabhavi, T.M. (2008) Synthesis, Characterization and Gas Permeability of an Activated Carbon-Loaded PEBAX 2533 Membrane. *Des. Monomers Polym.,* 11: 17-27. doi:10.1163/156855508X292392

140. Nasir, R., Mukhtar, H., Man ,Z., Shaharun, M.S., and Abu Bakar, M.Z. (2015) Effect of Fixed Carbon Molecular Sieve (CMS) Loading and various Di-Ethanolamine (DEA) Concentrations on the Performance of a Mixed Matrix Membrane for CO2/CH4 Separation. *RSC Adv.,* 5: 6814-6822. doi:10.1039/c5ra09015f

141. Guo, B., Tay, S.W., Liu, Z., and Hong, L. (2012) Assimilation of Highly Porous Sulfonated Carbon Nanospheres into Nafion® Matrix as Proton and Water Reservoirs. *Int. J. Hydrogen Energy,* 37: 14482-14491. doi:10.1016/j.ijhydene.2012.07.112

142. Tsai, L., Chien, H., Wang, C., Lai, C., Lin, J., Zhu, C., and Chang, F. (2013) Poly(Ethylene Glycol) Modified Activated Carbon for High Performance Proton Exchange Membrane Fuel Cells. *Int. J. Hydrogen Energy,* 38: 11331-11339. doi:10.1016/j.ijhydene.2013.06.054

143. Chien, H., Tsai, L., Lai, C., Lin, J., Zhu, C., and Chang, F. (2013) Characteristics of High-Water-Uptake Activated Carbon/Nafion Hybrid Membranes for Proton Exchange Membrane Fuel Cells. *J. Power Sources,* 226: 87-93. doi:10.1016/j.jpowsour.2012.10.017

144. Chai, Z., Wang, C., Zhang, H., Doherty, C.M., Ladewig, B.P., Hill, A.J., and Wang, H. (2010) Nafion-Carbon Nanocomposite Membranes Prepared using Hydrothermal Carbonization for Proton-Exchange-Membrane Fuel Cells. *Adv. Funct. Mater.,* 20: 4394-4399. doi:10.1002/adfm.201001412

145. Bhalara, P.D., Punetha, D., and Balasubramanian, K. (2014) A Review of Potential Remediation Techniques for Uranium(VI) Ion Retrieval from Contaminated Aqueous Environment. *J. Environ. Chem. Eng.,* 2: 1621-1634. doi:10.1016/j.jece.2014.06.007

146. Pal, P. and Kumar, R. (2014) Treatment of Coke Wastewater: A Critical Review for Developing Sustainable Management Strategies. *Sep. Purif. Rev.,* 43: 89-123. doi:10.1080/15422119.2012.717161

147. Sani, N., Lau, W. and Ismail, A. (2015) Morphologies and Separation Characteristics of Polyphenylsulfone-Based Solvent Resistant Nanofiltration Membranes: Effect of Polymer Concentration in Casting Solution and Membrane Pretreatment Condition. *Korean J. Chem. Eng.,* 32: 743-752. doi:10.1007/s11814-014-0281-2

148. Yam-Cervantes, M.A., Santiago-García, J.L., Loria-Bastarrachea, M.I., Duarte-Aranda, S., Alberto Ruiz-Trevino, F., and Aguilar-Vega, M. (2017) Sulfonated Polyphenylsulfone Asymmetric Membranes: Effect of Coagulation Bath (Acetic acid-NaHCO3/Isopropanol) on Morphology and Antifouling Properties. *J. Appl. Polym. Sci.,* 134: 44502. doi:10.1002/app.44502

149. Yuan, W., and Zydney, A.L. (2000) Humic Acid Fouling during Ultrafiltration. *Environ. Sci. Technol.,* 34: 5043-5050. doi:10.1021/es0012366

150. Guo, W., Ngo, H., and Li, J. (2012) A Mini-Review on Membrane Fouling. *Bioresour. Technol.,* 122: 27-34. doi:10.1016/j.biortech.2012.04.089

151. Roy, A. and De, S. (2017) State-of-the-Art Materials and Spinning Technology for Hemodialyzer Membranes. *Sep. Purif. Rev.,* 46: 216-240. doi:10.1080/15422119.2016.1256323

152. Vinh-Thang, H., and Kaliaguine, S. (2013) Predictive Models for Mixed-Matrix Membrane Performance: A Review. *Chem. Rev.,* 113: 4980-5028. doi:10.1021/cr3003888

153. Robeson, L.M. (2008) The Upper Bound Revisited. *J. Membr. Sci.,* 320: 390-400. doi:10.1016/j.memsci.2008.04.030

154. Chuah, C.Y., Goh, K., Yang, Y., Gong, H., Li, W., Karahan, H.E., Guiver, M.D., Wang, R., and Bae, T.H. (2018) Harnessing Filler Materials for Enhancing Biogas Separation Membranes. *Chem. Rev.,* 118: 8655-8769. doi:10.1021/acs.chemrev.8b00091

155. Fu, X.Y., Sotani, T., and Matsuyama, H. (2008) Effect of Membrane Preparation Method on the Outer Surface Roughness of Cellulose Acetate Butyrate Hollow Fiber Membrane. *Desalination,* 233: 10-18. doi:10.1016/j.desal.2007.09.022

156. Ahmadi, M., Janakiram, S., Dai, Z., Ansaloni, L., and Deng, L. (2018) Performance of Mixed Matrix Membranes Containing Porous Two-Dimensional (2D) and Three-Dimensional (3D) Fillers for CO2 Separation: A Review. *Membranes,* 8: 50. doi:10.3390/membranes8030050

157. Scholes, C.A., Stevens, G.W., and Kentish, S.E. (2012) Membrane Gas Separation Applications in Natural Gas Processing. *Fuel,* 96: 15-28. doi:10.1016/j.fuel.2011.12.074

158. Bakangura, E., Wu, L., Ge, L., Yang, Z., and Xu, T. (2016) Mixed Matrix Proton Exchange Membranes for Fuel Cells: State of the Art and Perspectives. *Prog. Polym. Sci.,* 57: 103-152. doi:10.1016/j.progpolymsci.2015.11.004

159. Ahmed, M.J.K., Ahmaruzzaman, M. (2016) A Review on Potential Usage of Industrial Waste Materials for Binding Heavy Metal Ions from Aqueous Solutions. *J. Water Process Eng.,* 10: 39-47. doi:10.1016/j.jwpe.2016.01.014

160. Tan, X., Liu, S., Liu, Y., Gu, Y., Zeng, G., and Hu, X. (2017) Biochar as Potential Sustainable Precursors for Activated Carbon Production: Multiple Applications in Environmental Protection and energy Storage. *Bioresour. Technol.,* 227: 359-372. doi:10.1016/j.biortech.2016.12.083

161. Gonzo, E.E., Parentis, M.L., and Gottifredi, J.C. (2006) Estimating Models for Predicting Effective Permeability of Mixed Matrix Membranes. *J. Membr. Sci.,* 277: 46-54. doi:10.1016/j.memsci.2005.10.007

162. Ji, W., Sikdar, S.K., and Hwang, S. (1995) Sorption, Diffusion and Permeation of 1,1,1-Trichloroethane through Adsorbent-Filled Polymeric Membranes. *J. Membr. Sci.,* 103: 243-255. doi:10.1016/0376-7388(95)00007-Y

163. Jusoh, N., Yeong, Y.F., Chew, T.L., Lau, K.K., and Shariff, A.M. (2016) Current Development and Challenges of Mixed Matrix Membranes for CO2/CH4 Separation. *Sep. Purif. Rev.,* 45: 321-344. doi:10.1080/15422119.2016.1146149

164. Brettmann, B.K., Tsang, S., Forward, K.M., Rutledge, G.C., Myerson, A.S., and Trout, B.L. (2012) Free Surface Electrospinning of Fibers Containing Microparticles. *Langmuir,* 28: 9714-9721. doi:10.1021/la301422x

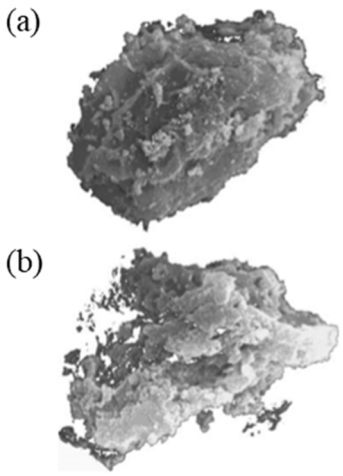

Figure 1: Particle breakage due to solvent etching of formed pores post activation of a 15 micron AC, (a) before, and (b) after contact with dimethylformamide (84). Reprinted with permission from Elsevier.

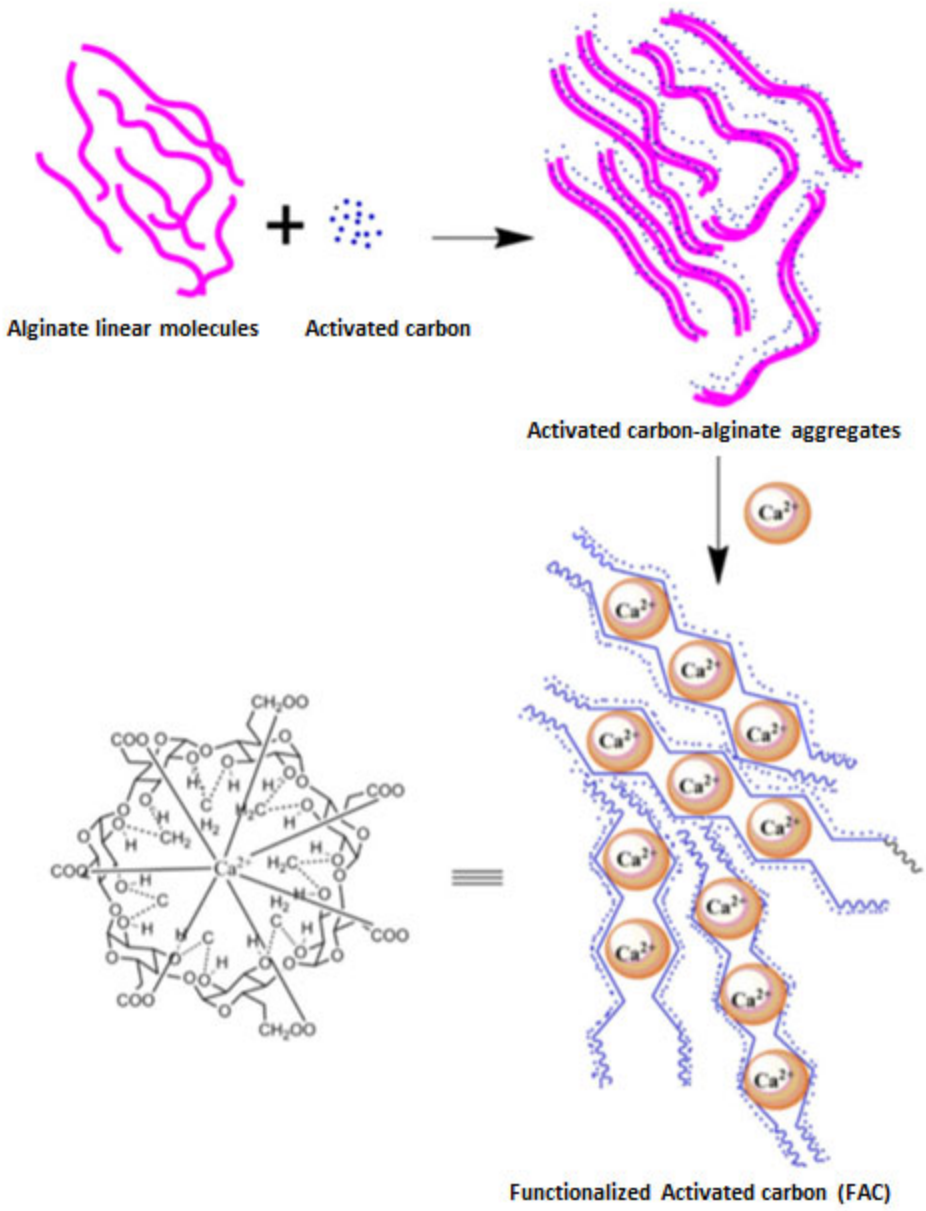

Figure 2: Schematic representation of AC functionalized with alginate by an ionic polymerization method and cross linked with calcium by the dissolution of calcium chloride in water (99). Reprinted with permission from Wiley.

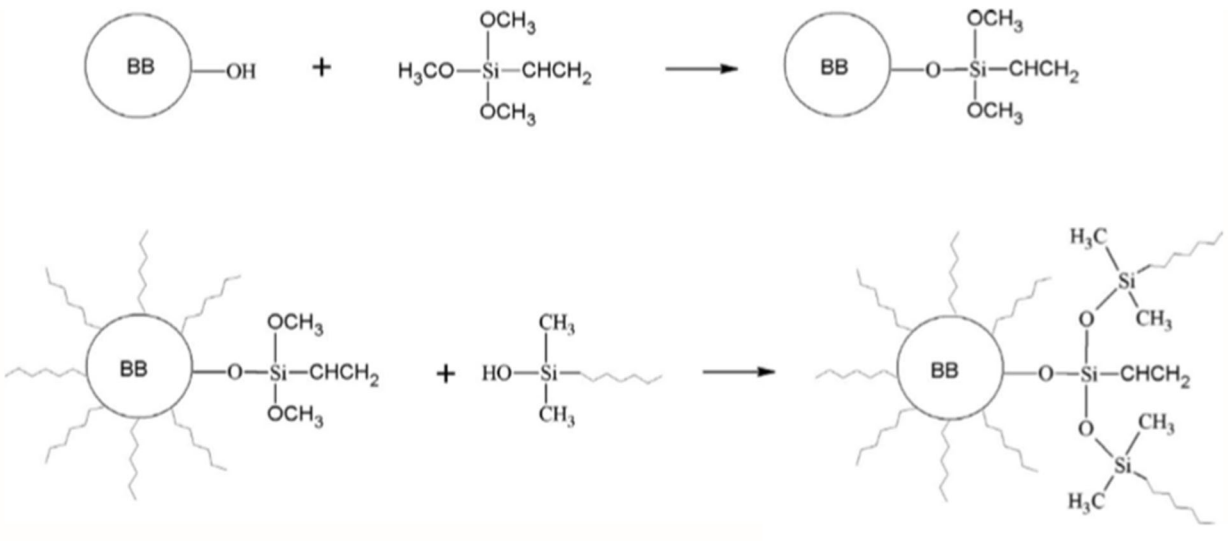

Figure 3: Proposed reaction between grafted biochar with PDMS resulting in highly hydrophobic membranes. Biochars (BB) were grafted with either YDH-171 (hydrophobic) or KH550 (slightly hydrophilic) (95). Reprinted with permission from Wiley.

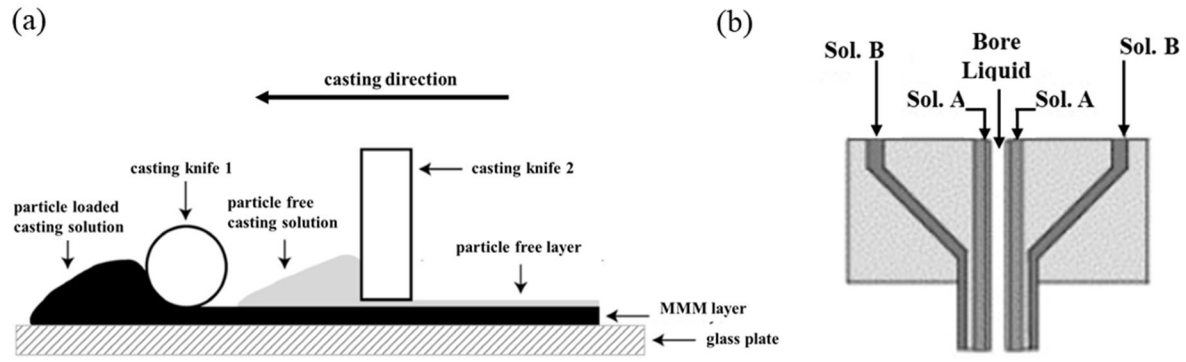

Figure 4: Schematic diagrams of multilayer casting apparatuses. Co-casting blade for (a) flat sheets (111) and multi-nozzle spinneret for (b) hollow fibers (113). Reprinted with permission from Elsevier.

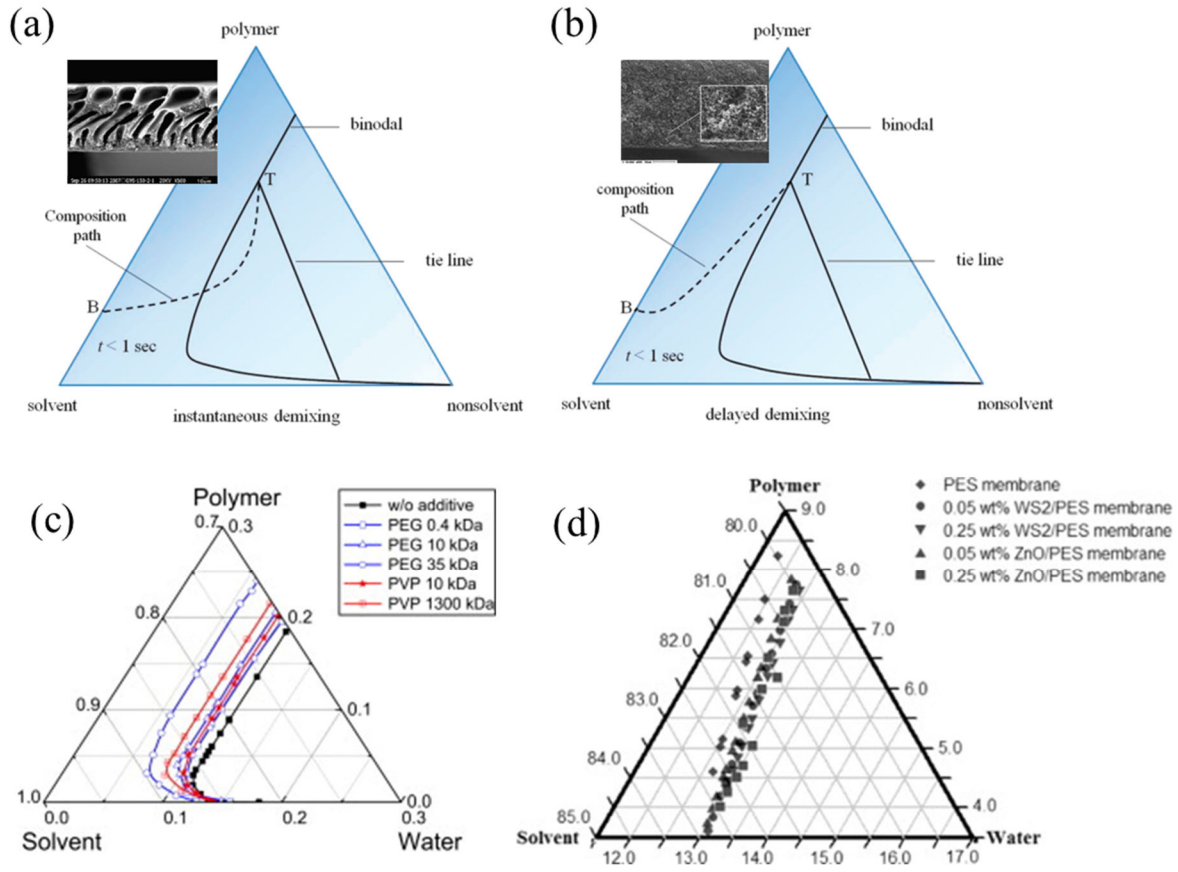

Figure 5: Ternary phase diagram showing (a) instantaneous demixing and the resulting finger-like morphology (108,114) (b) delayed demixing and the resulting spongy morphology (108,115) (c) the influence of PEG additives on binodal position (116) (d) the influence of metal particle additives on binodal position (117). Reprinted with permission from (a,b) ACS and (c,d) Elsevier.

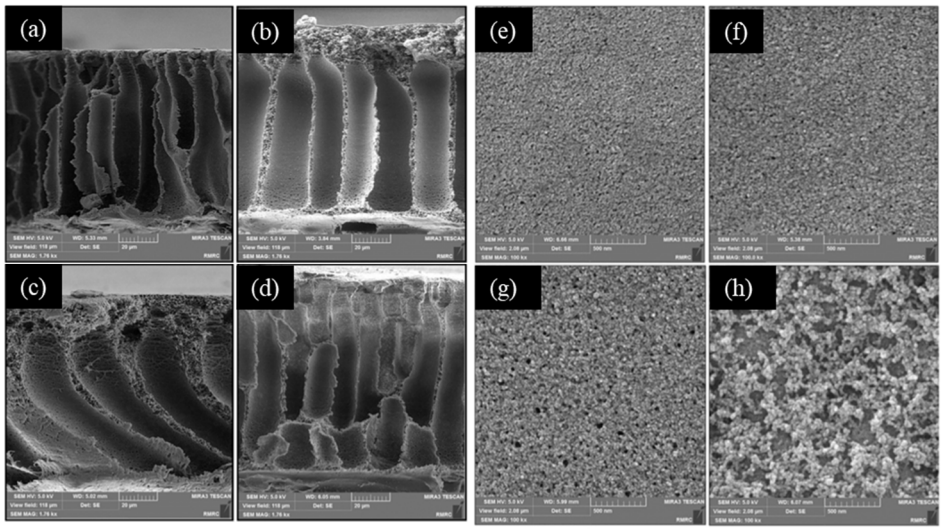

Figure 6: Triton-X results in finger like structure however, this finger like structure breaks down and surface becomes more porous with increasing amounts of AC from (a,e) 0 wt.%, (b,f) 0.1 wt.%, (c,g) 0.5 wt.%, and (d,h) 1 wt.%. (121). Reprinted with permission from Elsevier.

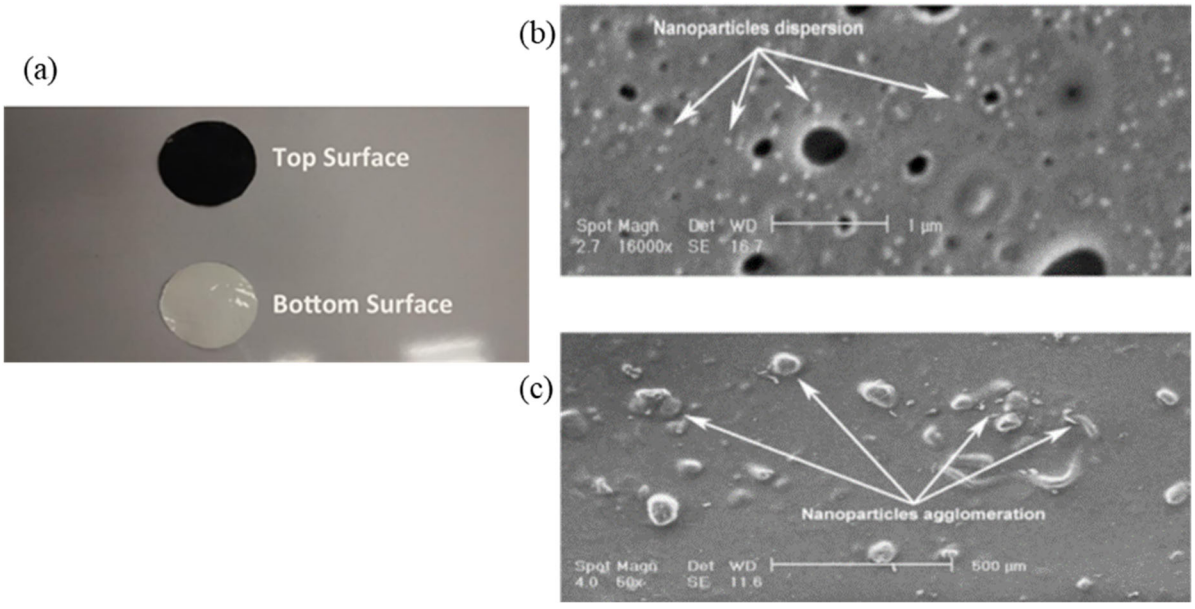

Figure 7: Migration of hydrophobic AC to the top surface occurs during wet phase inversion. (a) Macroscopic view showing black AC more apparent on the top view. (b) SEM image showing AC dispersion and pores on the bottom side with (c) High concentrations of agglomerations on the top side (123). Reprinted with permission from Elsevier.

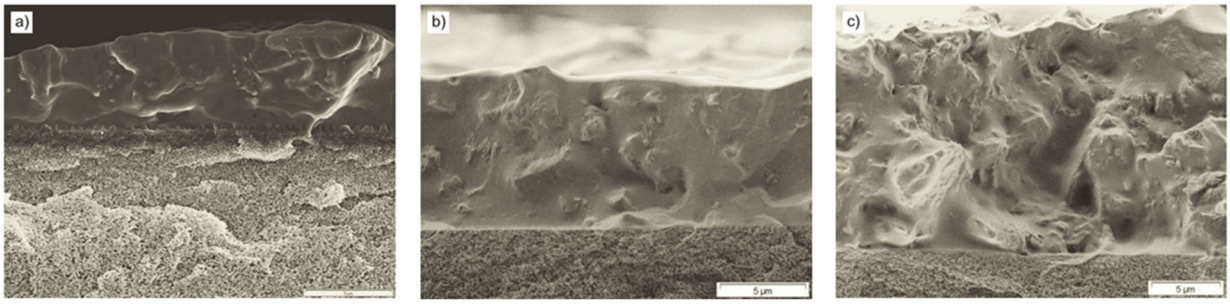

Figure 8: POMS membranes formed with AC loaded with (a) 10 wt.% (b) 20 wt.% (c) 40 wt.% showing the increase in inhomogeneity with increasing amounts of AC (89). Reprinted with permission from Wiley.

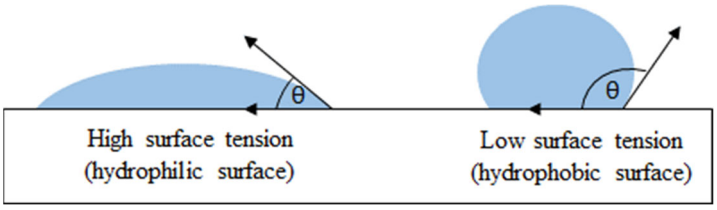

Figure 9: Example of the relationship between contact angle, surface tension, and hydrophilicity of membrane surfaces.

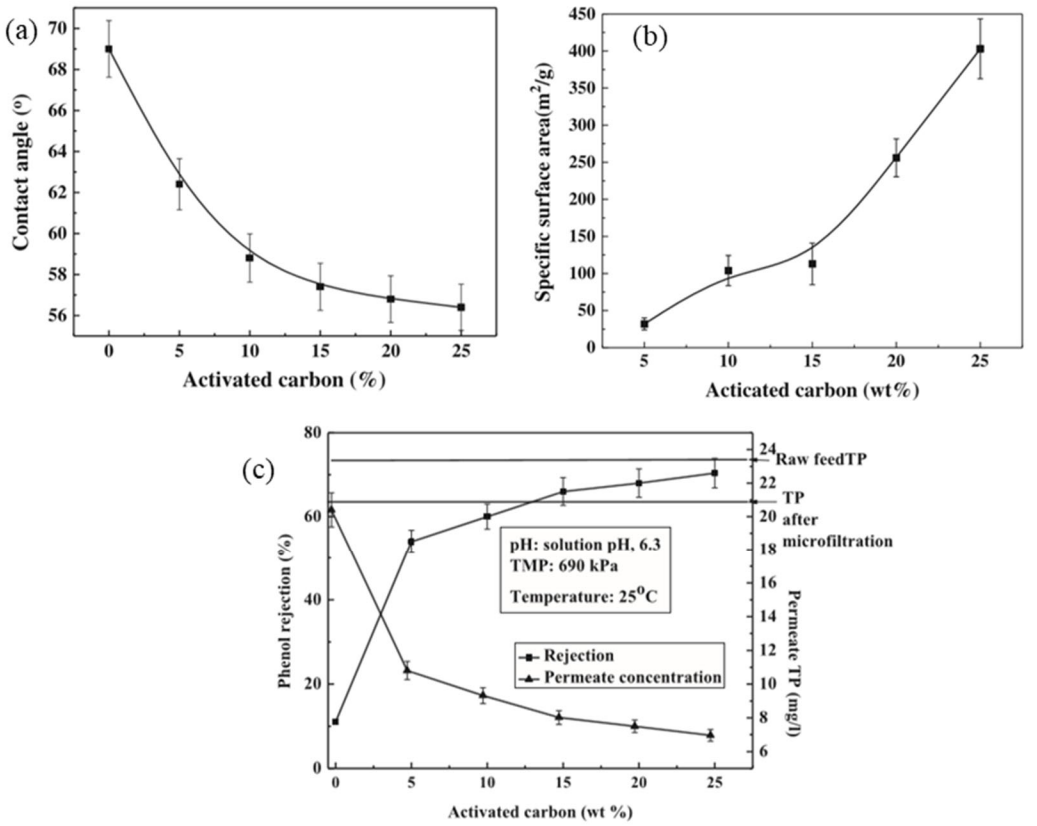

Figure 10: Influence of nano sized AC on (a) contact angle, (b) specific surface area, and (c) phenol rejection on an AC-CAP MMM (91). TP is the total phenol concentration. The secondary y-axis in (c) demonstrates the raw feed TP, TP after microfiltration with unloaded membranes, and the permeate TP using various loadings of AC. The steep decline from 23 TP in raw feed to 21 TP after microfiltration to 7 TP in the 25 wt.% AC-MMMs demonstrate the improved rejection performance. Reprinted with permission from Wiley.

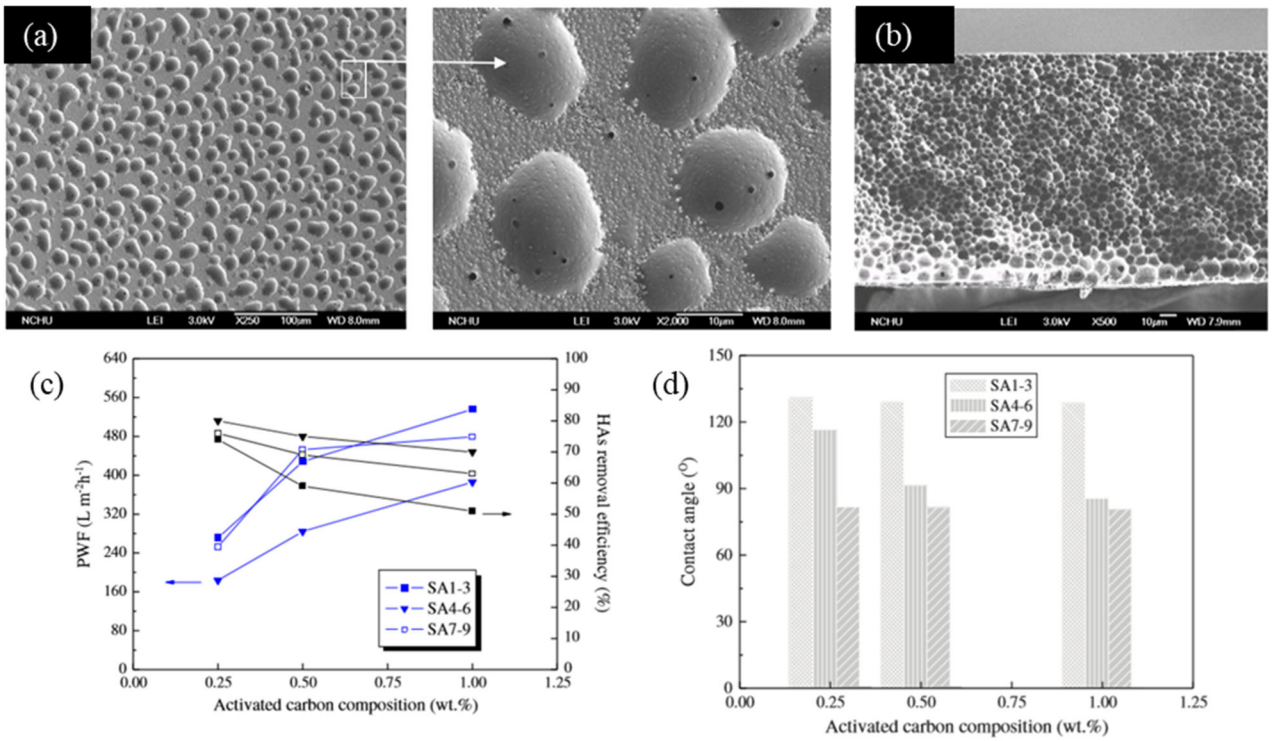

Figure 11: (a) Crater-like morphology formed on the tope surface of PEI-PPSU blended AC-MMM and the resulting (b) cross section. The influence of AC on (c) PWF and humic acid removal efficiency and (d) contact angle. Membranes were formed with 35 wt.% PPSU and 5 wt.% PEI. PEG pore forming agent was not used in samples SA1-3, 6 wt.% was added to SA4-6, and 12 wt.% to SA7-9. Each series of samples contains 0.25, 0.5, and 1 wt.% AC (120). Reprinted with permission from Elsevier.

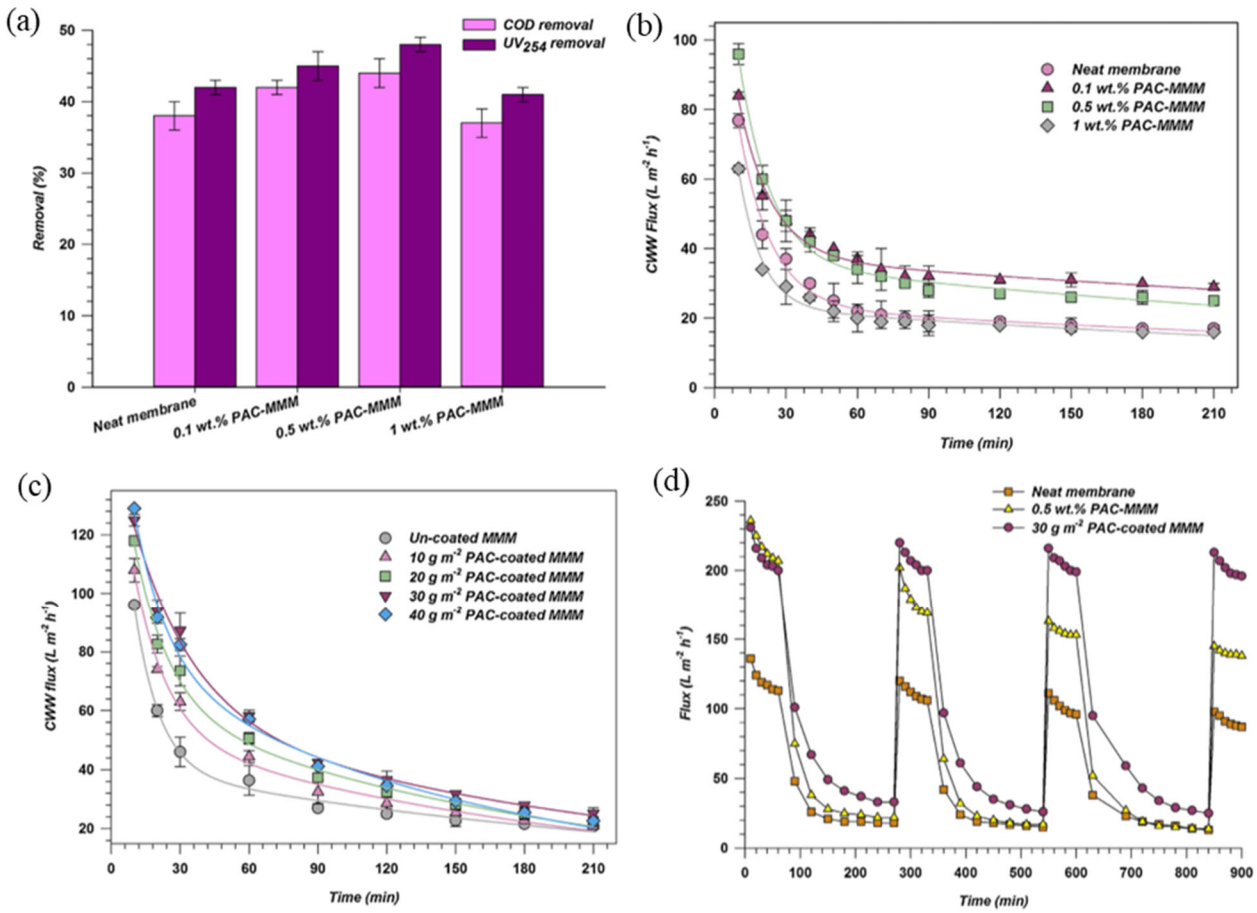

Figure 12: Influence of AC on (a) organic solute removal and (b) clean water flux over time. The influence on coated AC-MMMs on (c) clean water flux over time, and (d) improved regeneration ability (121). Reprinted with permission from Elsevier.

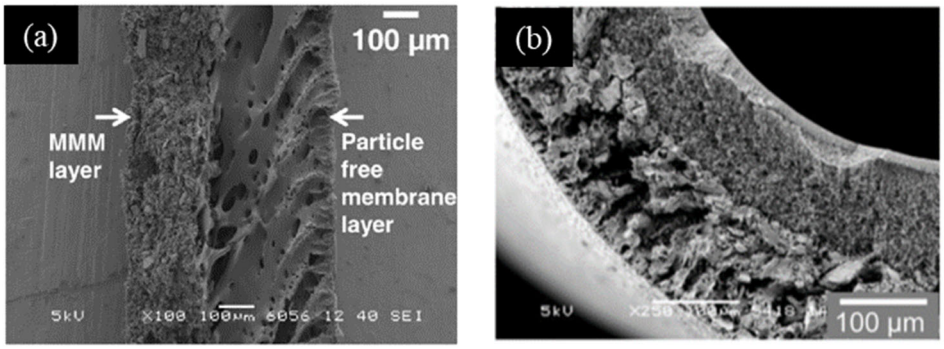

Figure 13: Two layer PES-PES/AC (a) flat sheet and (b) hollow fiber membranes (112). Reprinted with permission from Elsevier.

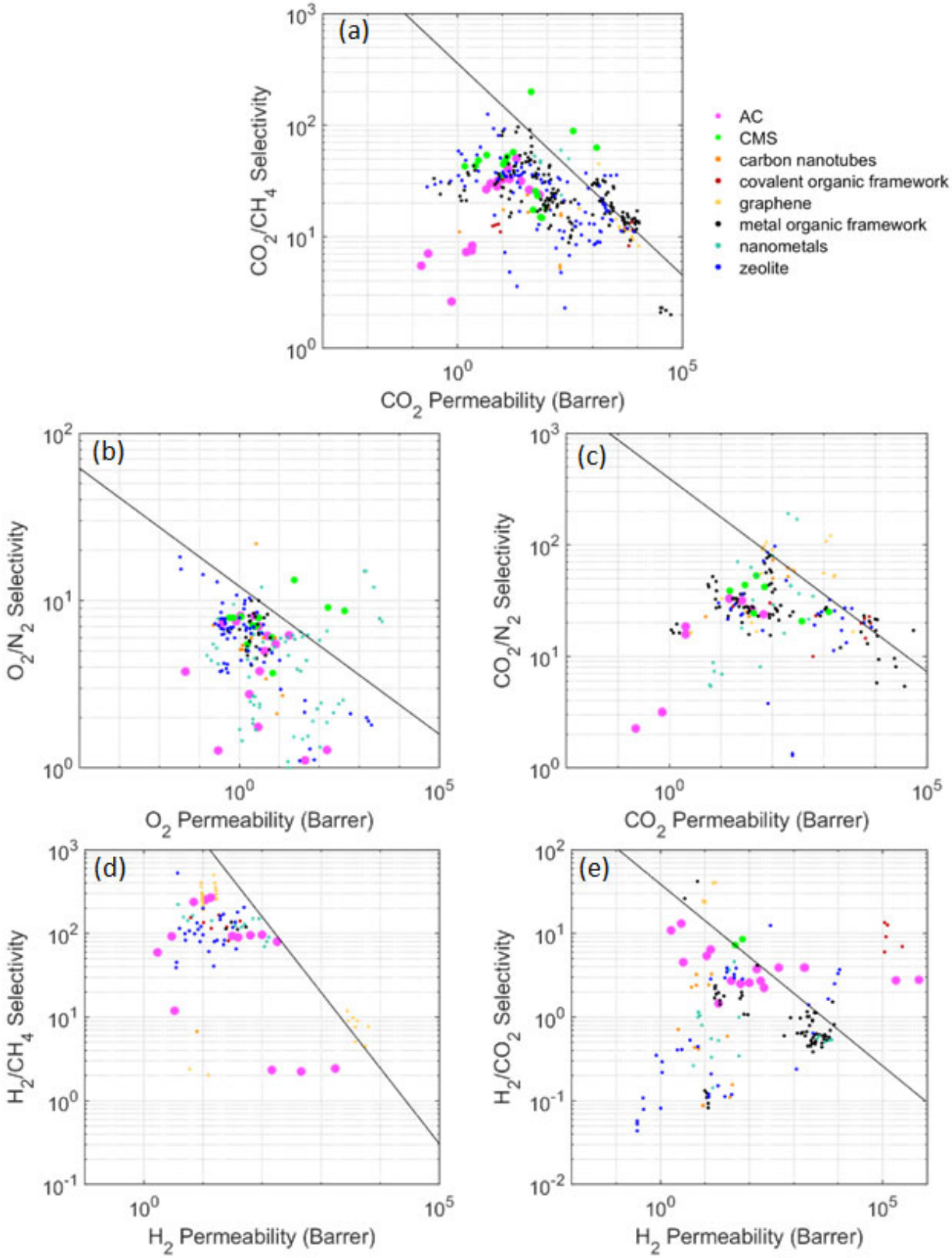

Figure 14: AC and CMS MMMs compared to other MMMs grouped by filler type for (a) CO_2/CH_4, (b) O_2/N_2, (c) CO_2/N_2, (d) H_2/CH_4, and (e) H_2/CO_2 gas pairs plotted against Robeson's 2008 upperbounds.

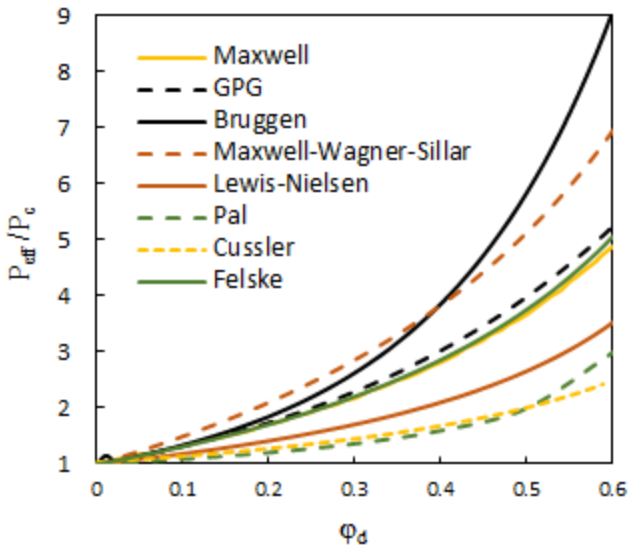

Figure 15: Comparative example of models with $P_c = 20$ and $P_d = 1000$, corresponding to $\beta = 0.94$. Other reasonable assumptions used are: $n = 0.2$, $\alpha = 5$, $\alpha_f = 10$, $\varphi_m = 0.5$, $P_I = 800$, $\delta = 1.01$.

Table 1: General comparison of different membranes in terms of their advantages/disadvantages in relation to the emerging class of MMMs.

Membrane	Advantages	Disadvantages
Polymeric Membranes (28,29) Ex: polysulfone, polyimide, polyethersulfone	• Easy synthesis and fabrication • Low production cost • Good mechanical stability • Easy upscaling and modeule design • Separation mechanism: Solution diffusion	• Low chemical and thermal stability • Plasticization • Pore size difficult to control • Permeability/selectivity trade off
Inorganic Membranes (30) Ex: Titanium oxide, zeolite, metal organic frameworks	• Superior chemical, mechanical, and thermal stability • Tunable pore size • Moderate permeability/selectivity trade off • Stable in harsh conditions • Separation mechanism is dependent on pore size: molecular sieving, surface diffusion, capillary condensation, Knudsen diffusion	• Brittle • Expensive • Difficult to scale up
Organic Membranes Ex: Carbon nanotubes(31), graphene (32)	• Tunable functional groups • Tunable pore size • Exceptional rejection in liquid separations • Moderate permeability/selectivity tradeoff • Separation mechanism: molecular sieving	• Difficult and expensive to make • Difficult to scale up • Can be frail
Mixed matrix membranes Ex: Matrimid-AC (10), PES-Kaolin (33), PVA-carboxyfullerene (34), PSF-MOF1 (35)	• Enhanced mechanical and thermal stability • Reduced plasticization • Low energy requirements • Surpasses permeability/selectivity trade off • Reduced fouling • Separation mechanism determined by the combined polymeric and filler properties	• Become brittle with high filler loadings • Poor interaction between matrix and filler results in unselective pores • Chemical and thermal stability depends on matrix material

Table 2: Properties of various biochars and their corresponding pyrolysis conditions. The pyrolysis type (fast/slow) is listed in the case exact heating rate was not listed.

Biochar Feedstock	**Surface Functional Groups**	**Surface Area (m^2/g)**	**Pyrolysis Temperature and Heating Rate**
Guinea Fowl Manure (50)	Hydrogen bonded, aliphatic amines	60.0	250°C – 2°C/min then 500°C – 5°C/min
Sugarcane Bagasse (51)	phenolic acids, carboxylic acids, lactonic acids	92.30	500°C, slow
Orange Peels (51)	phenolic acids, carboxylic acids, lactonic acids	0.21	500°C, slow
Sunflower seed hull (52)	Alcohols, amines, aromatic	3.850	450°C, fast
Bamboo (45)	Hydroxyl, carbonyl	332.10	600°C , slow
Date Palm (53)	Carbonyl, carboxylic acids	-	300-800°C, 5°C/min
Sewage Sludge (54)	Carbonyl, protonated	54.05	700°C , 25°C/min
Rice Husk (55)	Alcohols, phenol, carbonyl	27.8	350°C, 25°C/min
Dairy manure (55)	Hydroxyl, carbonyl, phosphate, aromatics	5.61	350°C, 25°C/min
Coconut coir (56)	Carboxylic acids, phenolic acids, hydroxyl	153	500, slow
Peanut Shells (46)	Carbonyl, aromatic, aromatic amines	420	700°C, 7°C/min
Soybean Stover (46)	Carbonyl, aromatic, aromatic amines	448	700°C, 7°C/min
Maple Wood (57)	Deprotonated carboxyl and phenolic acids	225	500°C, 2.5°C/min
Eucalyptus saw dust (58)	Carboxylic, hydroxyl	1.57	120°C, slow
Swine Manure (59)	Hydroxyl, carboxylic	3.46	400°C, 25°C/min
Rice Straw (59)	Carbonyl, hydroxyl	2.01	400°C, 25°C/min
Corncob (60)	Carbonyl, nitro, hydroxyl, methoxyl	3.38	15°C/min , 550°C
Potato Peel (61)	Carbonyl, hydroxyl, aromatics	2.29	700°C, 2°C/min
Pine Needle (47)	Hydroxyl, carbonyl, aromatics	390.52	700°C, 7°C/min
Almond Shell (62)	Carbonyl, phenols, lactones	30.35	650°C, 10°C/min

Table 3: Chemically activated AC produced from biochar and their processing conditions and resulting properties

Feed Stock	Activating Agent	Impregnation Ratio (agent: biochar)	Carbonization Temperature	Surface Area (m^2/g)	Functional Groups
Spruce Whitewood (67)	KOH	3.5 : 1	475°C 675°C 875°C	643 1317 2024	Hydroxyl, aromatics
Palm Date Seed (68)	NaOH	3:1	600°C	1282.49	Carbonyl, ketones, ethers, nitro
Coconut Shell (69)	H_2SO_4	1.5 : 1	600°C	-	Hydroxyl, carbonyl, ethers, aromatics
Grape Bagasse (70)	H_3PO_4	3:1	400°C 500°C 600°C	1021 909 629	Carbonyl, esters, ketones, aliphatic acids
Grape Stalk (71)	$ZnCl_2$	0.5: 1 1:1 1.5: 1 2:1	700°C	482.22 889.62 1004.48 1411.75	Hydroxyl, aromatics
Rice Husk (72)	KOH	5:1	750°C 850°C 950°C	2121 2696 1592	Hydroxyl, aromatics, ethers, esters
Sugar Cane Bagasse (73)	$ZnCl_2$	2:1	500°C	2200	Hydroxyl, carbonyl, aromatics
Sunflower Hulls (73)	$ZnCl_2$	2:1	600°C	1950	Hydroxyl, carbonyl, aromatics
Poplar Saw Dust (74)	KOH	1: 0.05	600°C	1506.2	Hydroxyl, carbonyl, carboxylic acids
Paulownia Wood (75)	H_3PO_4	4:1	400°C	2806	Carbonyl, aromatics, ketones, lactone, carboxyl, phosphates
Pork Bones (76)	H_2SO_4	2.8 : 1	800°C	110.7	Phosphates, carbonates

Table 4: Comparative properties of membranes produced by different phase inversion methods.

Inversion Method	Surface Morphology	Cross Sectional Morphology
Wet	Dense surface unless high filler content or pore forming agents are used.	Asymmetric with dense top skin and porous supporting layer. Porous layer can appear spongy, finger-like, or a combination of the two depending on inversion conditions.
Dry	Dense unless the evaporation rate is rapid, then surface pores can form. Filler materials can also cause ruptures leading to porous surfaces.	Dense and either homogeneous or asymmetric.
Dry/Wet	Dense or porous depending on the specific casting solution formation and conditions.	Dense or porous and asymmetric depending on the dry and wet phase steps. If the dry step dominated, the cross section will be denser than if the wet step dominates.

Table 5: Summary of most recent separation applications using AC-MM membranes with particular emphasis on the type of matrix used, AC source, method used for activating the derived carbon, and whether AC was commercial or synthesized in-house.

Matrix	**AC Precursor**	**Activating Method**	**AC Vendor**	**Application**	**Ref.**
PSF	Bagasse	Biochar was not activated	In house	Cu^{2+} and Pb^{2+} removal from water	(122)
PSF	Palm kernel shells	Not listed	Not listed	Ag^{+}, Pb^{2+}, Cd^{2+}, Cr^{3+} removal from water	(135)
PES	Bamboo	Not listed	US Research Nanomaterials, Inc., Houston, USA	Cu^{2+} and $(SO_4)^{2-}$ removal from water	(123)
PES	Polish subbituminous coal	Steam activation	In house	Cu^{2+} removal from water	(136)
CTA	Not listed	Not listed	Carbochem, LQ1000	Uranium removal from water	(137)
CTA	Not listed	Not listed	Norit NC-100	Uranium removal from water	(138)
PPSU	Acacia fumosa seed	HCl, functionalized with alginate	In house	Phenol removal from water	(99)
CAP	Not listed	Not listed	Merck (India) Ltd. Mumbai, India	Phenol removal from water	(91)
PSF	Not listed	Not listed	Merck (India) Ltd., Mumbai, India	Benzene, Toluene and Phenol, removal from water	(13)
PPSU	Coconut shell	Not listed	China Activated Carbon Industries Ltd., Taiwan	Humic acid removal from water	(120)
PSF	Broom sorghum	$ZnCl_2$	In house	Organic matter removal from cheese whey wastewater	(121)
CNF	Olive stones	KOH	In house	*E. coli.* removal from water	(78)
PES	Not listed	Not listed	Norit A Supra EUR, Norit Netherlands B.V., The Netherlands	Removal of creatinine from blood plasma	(111)
PES	Not listed	Not listed	Norit A Supra EUR, Norit Netherlands	Removal of creatinine, HA,	(112)

			B.V., The Netherlands	IS, and PCS from blood plasma	
PDMS	Not listed	Not listed	US1074 US-Nano Company SouthBend,IN,US	Pervaporation of butanol	(109)
PDMS	Tree biochar	Grafted with KH-550 and YDH-171	In house	Pervaporation of ethanol	(95)
ABS copolymer	not listed	Not listed	Maxsorb, The Kansai Coke & Chemical Co. Ltd. (Japan), Merk (Germany)	Separation of CO_2/CH_4	(15)
ABS	Not listed	Not listed	Not listed	Separation of CO_2/CH_4	(124)
PEBAX 2533	Not listed	Not listed	Permionics Membranes (Vadodara, India)	Separation of CO_2/CH_4	(139)
PEI	Not listed	Not listed	Maxsorb 3000, The Kansai Coke & Chemical Co. Ltd. (Japan)	H_2/CH_4, H_2/CO_2, H_2/O_2, H_2/N_2, CO_2/CH_4, O_2/N_2	(90)
PVC	Not listed	Not listed	Maxsorb 3000, The Kansai Coke & Chemical Co. Ltd. (Japan)	H_2/CH_4, H_2/CO_2, H_2/O_2, H_2/N_2, CO_2/CH_4	(102)
Matrimid	Not listed	Not listed	Blücher GmbH (Erkrath, Germany)	Pairs of He, H_2, O_2, N_2, CO_2, CH_4	(10)
PES	Not listed	Not listed	Aldrich	O_2/N_2	(92)
POMS	Not listed	Not listed	Blücher GmbH	n-C_4H_{10}/CH_4	(89)
POMS	Not listed	Not listed	Blücher GmbH	CO_2, C_2H_6, C_3H_8, n-C_4H_{10}, n-C_5H_{12}/CH_4	(79)
PES	Not listed	Not listed	Envior Chemical® Japan	CO_2/CH_4	(140)
Matrimid	Benzimidazole	Chemical crosslinking	In house	CO_2/N_2	(11)
Matrimid	Matrimid	Not Activated	In House	CO_2/CH_4 O_2/N_2	(7)
Nafion	Polypyrrole	KOH	In house	Methanol fuel cell	(141)
Nafion	Not listed	Post processed by acidification and PEG modification	Osaka Gas Co. Ltd.	Methanol fuel cell	(142,143)
Nafion	Glucose	steam	In house	Methanol fuel cell	(144)